

 Open access • Posted Content • DOI:10.1101/2021.08.02.454780

## **Arabidopsis Mediator subunit 17 connects transcription with DNA repair after UV-B exposure** — [Source link](#)

M. Giustozzi, S. Freytes, A. Jaskolowski, A. Jaskolowski ...+9 more authors

**Institutions:** National University of Rosario, Fundación Instituto Leloir, University of Lausanne, University of Buenos Aires ...+1 more institutions

**Published on:** 03 Aug 2021 - bioRxiv (Cold Spring Harbor Laboratory)

**Topics:** DNA repair, DNA damage, Arabidopsis, Gene and Transcription (biology)

Related papers:

- [Checkpoint-dependent phosphorylation of Med1/TRAP220 in response to DNA damage.](#)
- [p38γ regulates UV-induced checkpoint signaling and repair of UV-induced DNA damage](#)
- [Regulation and role of Arabidopsis CUL4-DDB1A-DDB2 in maintaining genome integrity upon UV stress.](#)
- [The nucleotide excision repair pathway is required for UV-C-induced apoptosis in Caenorhabditis elegans](#)
- [XPB induces C1D expression to counteract UV-induced apoptosis.](#)

Share this paper:    

View more about this paper here: <https://typeset.io/papers/arabidopsis-mediator-subunit-17-connects-transcription-with-4qribgcxq>

1 **Short Title: AtMED17 role during the DNA damage response**

2

3 **Author for Contact details: Paula Casati**

4

5 **Arabidopsis Mediator subunit 17 connects transcription with DNA repair after**  
6 **UV-B exposure**

7

8 **Marisol Giustozzi<sup>1</sup>, Santiago Nicolás Freytes<sup>2</sup>, Aime Jaskolowski<sup>2,5</sup>, Micaela**  
9 **Lichy<sup>2,6</sup>, Julieta Mateos<sup>2,7</sup>, Maria Lorena Falcone Ferreyra<sup>1</sup>, Germán L. Rosano<sup>3</sup>,**  
10 **Pablo Cerdán<sup>2,4</sup>, Paula Casati<sup>1,\*</sup>**

11

12 1. Centro de Estudios Fotosintéticos y Bioquímicos (CEFOBI), CONICET. Facultad de  
13 Ciencias Bioquímicas y Farmacéuticas, Universidad Nacional de Rosario, 2000  
14 Rosario, Argentina.

15 2. Fundación Instituto Leloir, IIBBA-CONICET, Buenos Aires, Argentina

16 3. Instituto de Biología Molecular y Celular de Rosario (IBR), CONICET, Facultad de  
17 Ciencias Bioquímicas y Farmacéuticas, Universidad Nacional de Rosario, 2000  
18 Rosario, Argentina.

19 4. Facultad de Ciencias Exactas y Naturales, Universidad de Buenos Aires, Buenos  
20 Aires, Argentina

21

22 **Current address:**

23 5. Department of Plant Molecular Biology, University of Lausanne, 1015 Lausanne,  
24 Switzerland.

25 6. IFEVA, Consejo Nacional de Investigaciones Científicas y Técnicas–Universidad de  
26 Buenos Aires, Buenos Aires, Argentina.

27 7. Universidad de Buenos Aires (UBA), Facultad de Ciencias Exactas y Naturales,  
28 Departamento de Fisiología, Biología Molecular y Celular and CONICET-UBA,  
29 Instituto de Fisiología, Biología Molecular y Neurociencias (IFIBYNE), (C1428EHA),  
30 Buenos Aires, Argentina.

31

32 \*Author for correspondence: Paula Casati. E-mail: [casati@cefobi-conicet.gov.ar](mailto:casati@cefobi-conicet.gov.ar). TE:  
33 +54 341 4371955

34

35 **One sentence summary:** In Arabidopsis, MED17 regulates the DNA damage response  
36 after UV-B exposure transcriptionally modulating the expression of genes and possibly  
37 also physically interacting with DNA repair proteins.

38

#### 39 **Author contributions**

40

41 M.G., P.Ce. and P.Ca. designed the research; M.G., S.N.F., A.J., M.L., J.M., M.L.F.F.,  
42 and G.R. performed the research; M.S., G.R., P.Ce. and P.Ca. analyzed and interpreted  
43 the data; and P.C. and M.G. wrote the manuscript.

44

45 The author responsible for distribution of materials integral to the findings  
46 presented in this article in accordance with the policy described in the Instructions for  
47 Authors (<https://academic.oup.com/plphys>) is: Paula Casati ([casati@cefobi-](mailto:casati@cefobi-conicet.gov.ar)  
48 [conicet.gov.ar](mailto:casati@cefobi-conicet.gov.ar)). The datasets generated and analyzed during this study are available  
49 from the corresponding author upon reasonable request.

50

#### 51 **Funding**

52 This research was supported by Argentina FONCyT grants PICT 2016-141 and 2018-  
53 798

54

55 **Abstract**

56 Mediator 17 (MED17) is a subunit of the Mediator complex that regulates  
57 transcription initiation in eukaryotic organisms. In yeast and humans, MED17 also  
58 participates in DNA repair, physically interacting with proteins of the Nucleotide  
59 Excision DNA Repair system. We here analyzed the role of MED17 in Arabidopsis  
60 plants exposed to UV-B radiation, which role has not been previously described.  
61 Comparison of *med17* mutant transcriptome to that of WT plants showed that almost  
62 one third of transcripts with altered expression in *med17* plants are also changed by UV-  
63 B exposure in WT plants. To validate the role of MED17 in UV-B irradiated plants,  
64 plant responses to UV-B were analyzed, including flowering time, DNA damage  
65 accumulation and programmed cell death in the meristematic cells of the root tips. Our  
66 results show that *med17* and *OE MED17* plants have altered responses to UV-B; and  
67 that MED17 participates in various aspects of the DNA damage response (DDR).  
68 Increased sensitivity to DDR after UV-B in *med17* plants can be due to altered  
69 regulation of UV-B responsive transcripts; but additionally MED17 physically interacts  
70 with DNA repair proteins, suggesting a direct role of this Mediator subunit during  
71 repair. Finally, we here also show that MED17 is necessary to regulate the DDR  
72 activated by ATR, and that PDCD5 overexpression reverts the deficiencies in DDR  
73 shown in *med17* mutants. Together, the data presented demonstrates that MED17 is an  
74 important regulator of the DDR after UV-B radiation in Arabidopsis plants.

75

76

## 77 **Introduction**

78 Mediator is a multi-subunit protein complex that regulates transcription initiation.  
79 Mediator acts as a molecular bridge between transcription factors bound at enhancers  
80 and RNA polymerase II (RNA pol II), but also regulates chromatin architecture, recruits  
81 epigenetic marks and participates in RNA processing. Structurally, Mediator is  
82 composed by four different modules, known as the head, middle, tail, and cyclin-  
83 dependent kinase 8 (CDK8) modules (reviewed in Buendía-Monreal and Gillmor, 2016;  
84 Malik et al., 2017; Mao et al., 2019). While the head module is thought to initially  
85 interact with RNA pol II to start transcription, the middle module has an important  
86 structural function and also binds to RNA pol II after its initial interaction with the  
87 head. The tail function is to associate with gene-specific transcription factors, whereas  
88 the CDK8 module is dissociable in response to different stimuli.

89 Even though the modular structure of the Mediator complex is conserved in  
90 eukaryotes, the composition of its subunits varies among species, but also changes in  
91 response to environmental and tissue-specific inputs, suggesting that different Mediator  
92 structures may have diverse functions (Mao et al., 2019). For instance, in plants, studies  
93 have shown that some Mediator proteins regulate cell division, cell fate and  
94 development, while others have a role in hormone signaling or are involved in biotic  
95 and abiotic stress responses. In plants, the Mediator complex comprises about 34  
96 subunits (Malik et al., 2017). Despite mutations in different Mediator subunits are not  
97 lethal, altered expression of particular MED subunits can lead to important changes in  
98 gene expression. Therefore, med mutants show different phenotypes, for example they  
99 have altered growth, development and stress responses (Yang et al., 2016; Dolan and  
100 Chapple, 2017). For example, Arabidopsis mutants in *MED5*, *MED16* and *MED23* have  
101 decreased accumulation of phenylpropanoid compounds (Stout et al., 2008; Dolan et al.,  
102 2017); *med16* mutants are deficient in cellulose biosynthesis and iron homeostasis  
103 (Sorek et al., 2015; Yang et al., 2014; Zhang et al., 2014), while in *med15* and *cdk8*  
104 plants, lipid biosynthesis is altered (Kim et al., 2006; Zhu et al., 2014; Kong and Chang,  
105 2018). Interestingly, several *med* mutants have shown contrasting metabolome profiles,  
106 which may relate to their different molecular function (Davoine et al., 2017).

107 MED17 is a subunit of the head Mediator module, and in the yeast and human  
108 complexes, it is an important protein which interacts with several other Mediator  
109 subunits (Guglielmi et al., 2004; Cevher et al., 2014). In Arabidopsis, MED17 seems to  
110 be a key scaffold component of the whole complex (Maji et al., 2019). AtMED17 was

111 demonstrated to participate in the production of small and long noncoding RNAs (Kim  
112 et al., 2011). MED17 is required for small RNA biogenesis recruiting Pol II to  
113 promoters of miRNA genes, and also for the repression of heterochromatic loci,  
114 activating Pol II-mediated production of long noncoding RNAs (Maji et al., 2019).  
115 These results suggest that MED17 may have a role not only in transcription but also in  
116 genome stability. In yeast, MED17 participates in DNA repair through a physical  
117 interaction with Xeroderma pigmentosum group G protein (XPG), an endonuclease that  
118 participates in Nucleotide Excision DNA Repair (NER; Eyboulet et al., 2013).  
119 Moreover, *med17* mutants show increased sensitivity to UV radiation. Thus, MED17  
120 participates in DNA repair recruiting XPG to transcribed genes (Eyboulet et al., 2013).  
121 In human cells, MED17 was shown to interact with the DNA helicase Xeroderma  
122 pigmentosum group B protein (XPB), which is a subunit of the transcription factor II H  
123 (TFIIH) and it is essential for both transcription and NER (Kikuchi et al., 2015).  
124 MED17 colocalizes with the NER factors XPB and XPG after UV-C exposure *in vivo*,  
125 and they also physically interact in *in vitro* assays, suggesting that, similarly as it was  
126 described in yeasts, MED17 plays essential roles in the switch between transcription  
127 and DNA repair (Kikuchi et al., 2015). The major DNA lesions that occur after UV  
128 exposure are the formation of cyclobutane pyrimidine dimers (CPDs) and pyrimidine  
129 (6-4) pyrimidones (6-4 PPs), which occur on two adjacent pyrimidine bases. In plants,  
130 these photoproducts are mainly repaired through photoreactivation, which is the direct  
131 reversal of major lesions by different types of photolyases that absorb light and reverse  
132 the formation of CPDs or 6-4 PPs (Spampinato, 2017). In Arabidopsis, UVR2 is a CPD  
133 photolyase, while UVR3 catalyzes the photoreactivation of 6-4 PPs. However, other  
134 DNA repair systems that are independent of light absorption, such as the NER system,  
135 which removes damaged nucleotides together with surrounding nucleotides; the Base  
136 Excision Repair (BER) system, which removes damaged bases, and other repair systems  
137 like the Mismatch Repair (MMR) system that recognizes and corrects of DNA  
138 mismatches have been also shown to repair DNA damage after UV exposure  
139 (Spampinato, 2017; Lario et al., 2011).

140 In this manuscript, we investigated the role of MED17 in Arabidopsis plants  
141 exposed to UV-B radiation. Using *med17* mutants, we analyzed their transcriptome and  
142 compared it to that of WT plants. Our results demonstrate that transcripts that encode  
143 proteins that participate in UV-B responses and DNA repair genes showed altered  
144 expression in *med17* mutants. *med17* mutants also showed altered phenotypes after

145 UV-B exposure, in particular during the DNA damage response. We here show that  
146 MED17 is necessary for the correct expression of genes after UV-B exposure, probably  
147 by interacting with other Mediator proteins and transcription factors, but it also binds  
148 proteins that participate in DNA repair in Arabidopsis, suggesting that MED17 may  
149 have a direct role during DNA repair. In addition, MED17 is required for DDR  
150 activation through Ataxia telangiectasia and Rad3 related (ATR); and overexpression of  
151 Programmed cell death 5 (PDCD5), a regulator of the DDR in humans and in  
152 Arabidopsis, overcomes the deficiency of responses to UV-B in *med17* mutants.  
153 Together, the data presented here demonstrates that MED17 is a key regulator of the  
154 DNA damage response after UV-B radiation in Arabidopsis plants.

155

156

157 **Results**

158

159 Transcriptome analysis of *med17* mutants

160

161 As MED17 is a subunit of the transcriptional co-regulator Mediator complex, we were  
162 first interested in studying the global role of MED17 on gene expression. Thus, we  
163 compared the transcriptome of *med17* mutants and WT seedlings grown under white  
164 light for 10 days. Three biological replicates were used for RNA extraction and RNA-  
165 seq analysis. We identified 6822 differentially expressed genes in *med17* mutants in  
166 comparison to WT plants (Figure 1, A; Supplemental Table S1), 3534 (51.8%) were  
167 downregulated, whereas 3288 (48.2%) were upregulated. MED17 responsive genes  
168 were enriched in GO terms related to red, far-red, blue and UV-B light responses,  
169 among others (Supplemental Table S2). These results suggested a possible role for  
170 MED17 in UV responses. As described in the Introduction, MED17 was reported to  
171 participate in DNA repair after UV exposure in yeast and humans. Therefore, we  
172 compared the transcriptome changes of *med17* mutants to those of Col-0 plants grown  
173 under white light in our experiments (Supplemental Figure S1) to those previously  
174 reported for Col-0 plants after UV-B exposure (Tavridou et al., 2020). As shown in  
175 Figure 1, A, out of the 5079 UV-B regulated transcripts in WT plants (Tavridou *et*  
176 *al.*, 2020), 2184 showed altered expression in *med17* mutants, which was significant  
177 by a Fisher Exact Test ( $p=4.6e-53$ ). Interestingly, 56% of this overlapping set of  
178 transcripts were up-regulated by UV-B in WT plants and down-regulated in *med17*  
179 mutants (Supplemental Figure S1, A), which was highly significant (Fisher Exact Test  
180  $p<1e-242$ ; Figure 1, D). The overlap between up-regulated genes in *med17* mutants and  
181 down-regulated in Col-0 plants by UV-B was also significant, although not to the same  
182 extent ( $p < 0.005$ ; Figure 1, D). On the other hand, the overlap between the other two  
183 possible comparisons (up by UV-B vs up by *med17*; down by UV-B vs down by *med17*  
184 was 26 % altogether, and not statistically significant (Figure 1, D). Furthermore, the  
185 Odds ratio, which represents the strength of the association or correlation of the overlap,  
186 was higher for genes that are increased by UV-B and decreased in *med17* than for all the  
187 other comparisons (Figure 1, D). These results show that the transcripts that increase in  
188 response to UV-B require MED17 for maximal expression in the WT, suggesting a role  
189 for MED17 in UV-B responses.



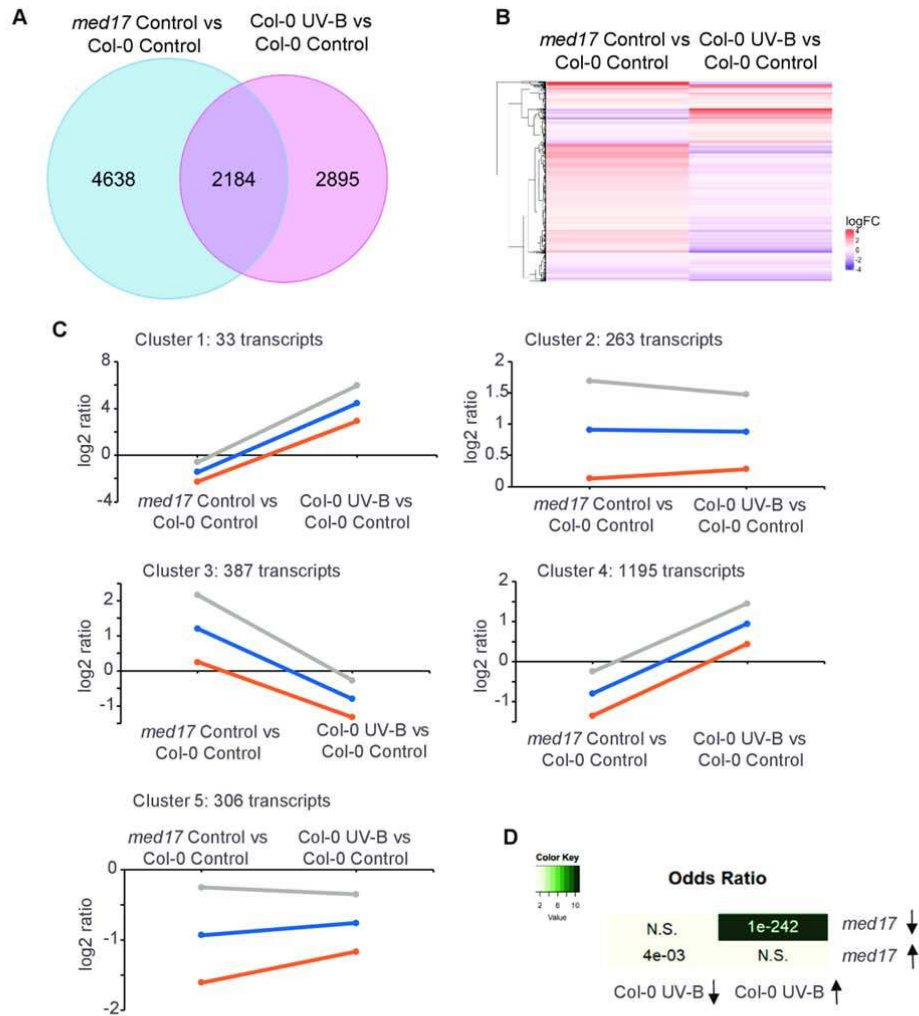


**Figure 1** Analysis of global gene expression differences between *med17* compared to WT plants grown without UV-B (Control), and WT plants exposed to UV-B radiation (UV-B) compared to non treated plants (Control). A, Venn diagram of comparisons between transcripts with altered expression in *med17* mutants and UV-B-responsive genes in Arabidopsis plants. Sets of genes were selected using the criteria described in Materials and methods. B, Heatmap comparing transcripts changed in *med17* compared to WT plants; and WT plants after UV-B exposure. The color saturation reflects the magnitude of the log2 expression ratio for each transcript. C, Clusters of expression profiles. Each graph displays the mean pattern of expression of transcripts in the cluster in blue and the standard deviation of average expression (orange and grey lines). The number of transcripts in each cluster is at the top left corner of each graph. The y-axis represents log2 of gene-expression levels relative to those in WT Col-0 plants under control conditions without UV-B. D, Fisher Exact Test and Odds Ratio of the overlap between differentially expressed transcripts in *med17* compared to WT plants and UV-B regulated transcripts in WT plants.

190 We then performed a cluster analysis of the 2184 overlapping genes shown in  
 191 the Heatmap (Figure 1, B. Figure 1, C, and Supplemental Table S2). Genes were  
 192 clustered in 5 groups, with clusters 1 and 4 including transcripts with decreased  
 193 expression in *med17* compared to WT plants grown under white light conditions, and  
 194 up-regulated by UV-B in Col-0 plants (Figure 1C). These two clusters mainly differ in  
 195 the magnitude of the change observed; cluster 1 includes a lower number of transcripts,

196 but showing stronger changes compared to WT plants, while cluster 4 includes more  
197 transcripts with smaller differences. Interestingly, when the clusters were analyzed by  
198 GO terms, cluster 1 included the categories UV-B responsive genes, flavonoid and  
199 secondary metabolites biosynthesis, and oxidoreduction reactions. This cluster contains  
200 highly upregulated genes in WT plants exposed to UV-B compared to plants under  
201 white light, but downregulated in *med17* mutants compared to Col-0, both grown in the  
202 absence of UV-B. Among genes included in cluster 1, we found *EARLY LIGHT-*  
203 *INDUCIBLE PROTEIN 2 (ELIP2)*, which was shown to be activated by UV-B through  
204 UVR8 (Brown, 2005), with a log<sub>2</sub> fold change of 6.39 in WT under UV-B, and -3.29 in  
205 *med17* plants (Supplemental Table S2). *REPRESSOR OF UV-B*  
206 *PHOTOMORPHOGENESIS 2 (RUP2)* was also found in this cluster. RUP2, along with  
207 RUP1, provides an UVR8 negative feedback regulation, balancing UV-B responses  
208 (Gruber, 2010). RUP2 showed a 3.20 log<sub>2</sub> fold change in WT exposed to UV-B, while  
209 *med17* plants showed a log<sub>2</sub> fold change of -1.45 (Supplemental Table S2). On the  
210 other hand, cluster 4 included GO terms related to light responses (light stimulus, high  
211 light, red, far-red, blue, photosynthesis), oxidative stress and response to reactive  
212 oxygen species, amongst others (Supplemental Table S2). Remarkably, in this cluster  
213 we found genes induced by UV-B like *DREB2A* (Ulm et al., 2004), and *RUP1*,  
214 mentioned above. This analysis further validates the requirement of MED17 for  
215 increased expression of genes that participate in UV-B responses.

216

217 Photomorphogenic responses are altered in *med17* mutants.

218

219 Because *med17* mutants had altered expression of some genes regulated by UV-  
220 B radiation, we studied UV-B responses in *med17* plants. First, we analyzed *med17*  
221 seedling lethality after UV-B exposure. Seedlings were grown on MS-agar plates under  
222 light conditions; a group of plants was irradiated with UV-B for 1h while a different  
223 group was kept in the dark for the same period. A third group of plants was grown  
224 under normal light conditions. Although *med17* seedlings germinated and grew similar  
225 to WT seedlings under white light illumination (100  $\mu\text{E m}^{-2}\text{s}^{-1}$ ); darkness affected the  
226 growth of some *med17* mutants. However, a UV-B treatment provoked lethality of most  
227 *med17* plants, while WT seedlings were very low affected by the same treatment  
228 (Figure 2, A).

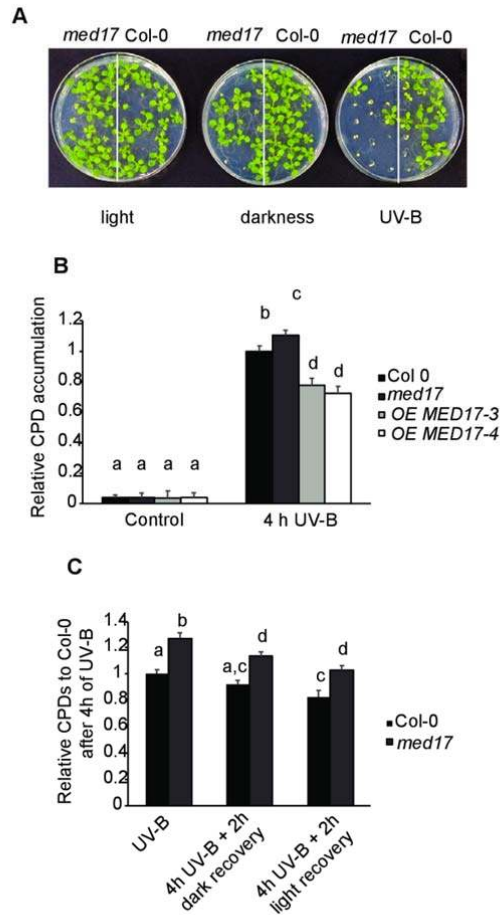


**Figure 2** *med17* plants show higher UV-B sensitivity and DNA damage after UV-B than WT plants. A, Representative images of *med17* and WT Col-0 seedlings grown under light conditions and after 15 days were UV-B irradiated (UV-B) or kept under dark conditions (darkness) as described in Materials and methods. Alternatively, plants were grown under normal photoperiod (light conditions, and then kept under normal growth conditions after UV-B or kept under dark conditions. B and C, Relative CPD levels in the DNA of WT Col-0, *med17* and OE MED17 plants grown under control conditions or immediately after a 4-h UV-B treatment under light conditions (B), or immediately after a 4-h UV-B treatment under dark conditions and 2 h after recovery in the dark or in the light to allow photorepair (C). Results represent averages  $\pm$  S.E.M. of six independent biological replicates. Different letters indicate statistically significant differences applying ANOVA test ( $P < 0.05$ ), asterisks indicate statistically significant differences applying T-Student test ( $P < 0.05$ ).

229                      Flowering time is delayed by UV-B radiation in Arabidopsis (Dotto et al., 2018;  
 230 Arongaus et al., 2018). As previously reported in Kim et al. (2011) and similarly as it  
 231 was also demonstrated for other Mediator subunit mutants such as *med25* and *med18*  
 232 (Iñigo et al., 2012; Zheng et al., 2013), *med17* mutants flowered later than WT plants  
 233 (Supplemental Figure S2, A-C). After growth under UV-B conditions, while WT plants  
 234 showed a delay in flowering time, *med17* mutants showed a similar flowering time as  
 235 that observed under control conditions. Thus, MED17 is a regulator of this  
 236 developmental pathway and it may have a role in the regulation of flowering time under

237 UV-B conditions. Together, the phenotypes analyzed show that *med17* mutants are  
238 sensitive to UV-B exposure.

239

240 Plants with altered expression of *MED17* are deficient in the DNA damage response.

241

242 We then focused on the role of *MED17* in the DNA damage response after UV-B  
243 exposure. We first investigated if *MED17* participates in DNA damage and repair using  
244 both *med17* mutants and transgenic plants that overexpress *MED17* under the control of  
245 the 35S promoter (*OE MED17*; Supplemental Figure S3). While all plants showed very  
246 low and similar levels of CPDs under control conditions in the absence of UV-B, *med17*  
247 mutants accumulated higher DNA damage after a UV-B treatment than WT plants when  
248 the treatments were done under conditions that allowed photoreactivation (Figure 2, B).  
249 On the contrary, *OE MED17* plants had less CPDs after UV-B exposure under the same  
250 conditions. *med17* mutants also accumulated more CPDs than WT plants when the UV-  
251 B treatments were done in the dark to prevent DNA repair by photolyases, and 2h after  
252 the end of the UV-B treatment, either when recovery was done under light or dark  
253 conditions (Figure 2, C). Thus, *med17* mutants accumulate more CPDs after UVB  
254 exposure, and *MED17* role during DNA damage and repair seems to be important not  
255 only during dark repair but also during photoreactivation.

256 We next analyzed whether plants with altered *MED17* expression showed  
257 differences in programmed cell death (PCD) after UV-B exposure. When DNA damage  
258 occurs, DNA damage responses (DDR) are triggered that converge to a PCD pathway,  
259 so as to avoid propagation of mutations in case the damage is not properly repaired  
260 (Furukawa et al., 2010). As shown in Figure 3, A, C, one day after a UV-B treatment,  
261 WT primary roots accumulated a higher number of dead cells after UV-B exposure than  
262 *med17* roots, and lower than *OE MED17* lines; while none of the analyzed lines showed  
263 any dead cells in untreated roots. However, 4 days after the treatment, although UV-B  
264 irradiated WT and *OE MED17* roots recovered and dead cells were almost undetectable;  
265 the number of dead cells in UV-B irradiated *med17* mutants was higher than in WT  
266 roots (Figure 3, B, C). Thus, *MED17* is required for a proper activation of the PCD  
267 pathway after UV-B exposure.

268 Another consequence of the DDR in plants is the inhibition of cell proliferation  
269 (Culligan et al., 2006). Thus, we analyzed the effect of UV-B on cell proliferation in the  
270 primary root meristems of plants with altered *MED17* expression. *med17* mutants had a

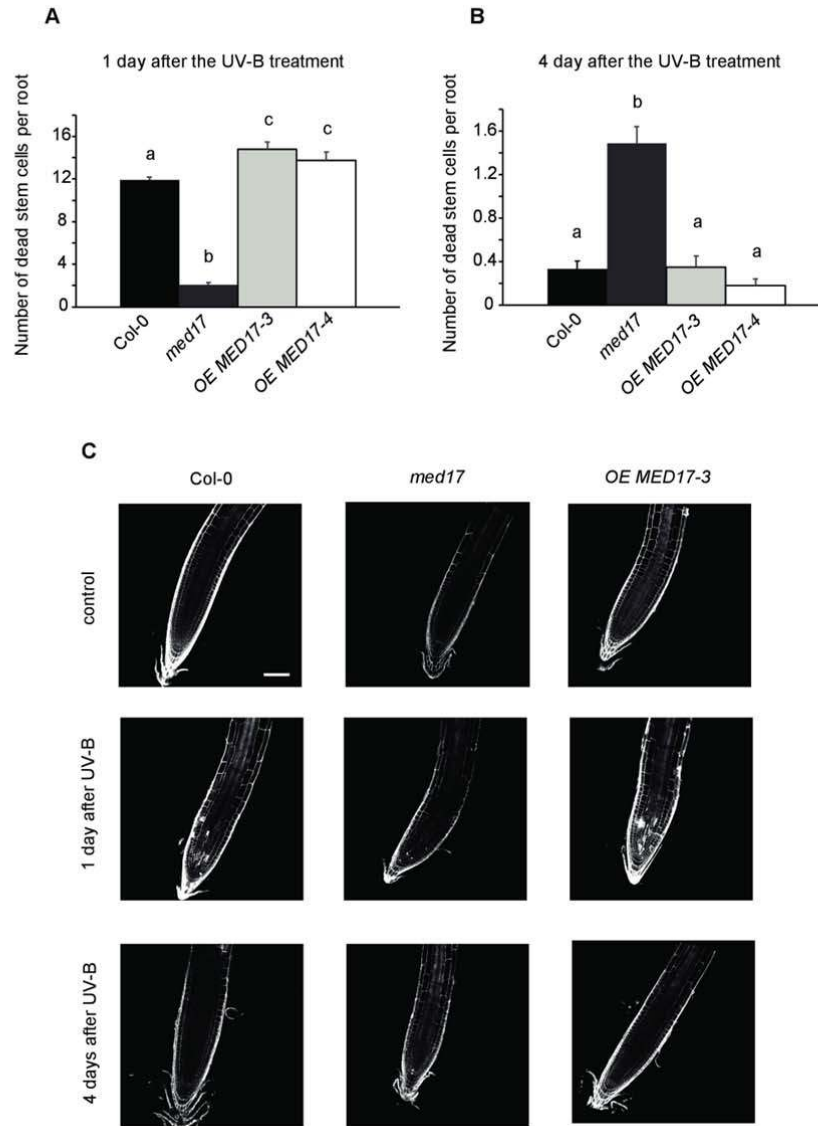


**Figure 3** Programmed cell death in meristematic root cells in WT Col-0, *med17* and *OE MED17* plants after UV-B exposure. A and B, Number of stem cells that are dead after 1 day (A) or 4 days (B) of UV-B exposure in WT Col-0, *med17* and *OE MED17* roots. Results represent the average of at least 50 biological replicates  $\pm$  S.E.M. Different letters indicate statistically significant differences applying analysis of variance test ( $p < 0.05$ ). C, Representative images of stem cells and adjacent daughter cells from WT Col-0, *med17* and *OE MED17* seedlings that were scored for intense PI staining to count dead stem cells per root 1 day and 4 days after a UV-B treatment or under control conditions. Scale bar represents 100  $\mu$ m.

271 smaller meristematic zone in the primary root than WT plants, which was significantly  
 272 decreased after a UV-B treatment (Supplemental Figure S4, A and 5). The decrease in  
 273 the meristematic zone size was higher in *med17* than in WT plants, in contrast to *OE*  
 274 *MED17* plants, which were less inhibited by UV-B (Supplemental Figure 4, A and B).  
 275 The higher decrease in the meristem size of *med17* roots by UV-B was a consequence  
 276 of a higher inhibition of cortex cell proliferation than that measured in WT roots; and  
 277 the opposite was observed in *OE MED17* roots (Supplemental Figure 4, C and D), while

278 the increase in cortex cell length determined in the meristems of all plants by UV-B was  
279 similar (Supplemental Figure 4, E and F). In this way, MED17 also regulates cell  
280 proliferation after UV-B exposure, altering root meristem size.

281

282 *med17* and *OE MED17* plants show altered UV-B regulation of gene expression

283

284 Next, we investigated how the expression of genes that respond to this radiation  
285 and regulate its responses was affected in *med17* seedlings after UV-B exposure. First,  
286 we analyzed the expression of three transcripts encoding enzymes that participate in  
287 DNA repair by UV-B, *UVR2* and *UVR3*, which encode CPD and 6-4 photoproduct  
288 photolyases, respectively; and *UVR7* (or *ERCC1*), which encodes a DNA repair  
289 endonuclease of the NER system. *UVR3* belongs to cluster 4 in Figure 1, C, showing  
290 decreased expression in *med17* plants (Supplemental Table S2). While the expression of  
291 *UVR2* was similar in *med17* and WT seedlings after UV-B exposure; *UVR3* and *UVR7*  
292 showed significantly lower levels than WT plants under control and UV-B conditions  
293 (Figure 4, A-C). Thus, the higher accumulation of CPDs by UV-B in *med17* plants  
294 could be due to decreased expression of DNA repair enzymes. As flowering time was  
295 also affected in *med17* plants, we analyzed the expression of *FLC*, which encodes a  
296 master repressor of flowering time (Michaels and Amasino, 1999). *FLC* levels were  
297 significantly higher in *med17* both under control conditions and after UV-B, with  
298 similar levels under both conditions (Figure 4, D); hence, the delay in flowering time in  
299 *med17* under both conditions could be explained by increased levels of this protein.  
300 Transcript levels of the DNA damage response kinases ATR and ATM, and the  
301 transcription factor SOG1, a master regulator of the DDR (Furukawa et al., 2010), were  
302 also analyzed. Fig 4, E-G, shows that both *ATR* and *ATM* levels were higher in *med17*  
303 than in WT plants, both under control conditions and after UV-B exposure. However,  
304 *SOG1* expression was significantly decreased in *med17* under both conditions analyzed,  
305 suggesting that decreased levels of this transcription factor may affect the DNA  
306 responses after UV-B exposure. On the contrary, *MAPK6* levels in *med17* mutants were  
307 not different to those in WT plants (Figure 4, H), this kinase is also a regulator of some  
308 UV-B responses, so the phenotypes observed in the mutants are not due to changes in  
309 the expression of this enzyme.

310 *UVR8*, which encodes the UV-B photoreceptor that regulates mostly  
311 photomorphogenic responses and which levels were not changed by UV-B in WT plants

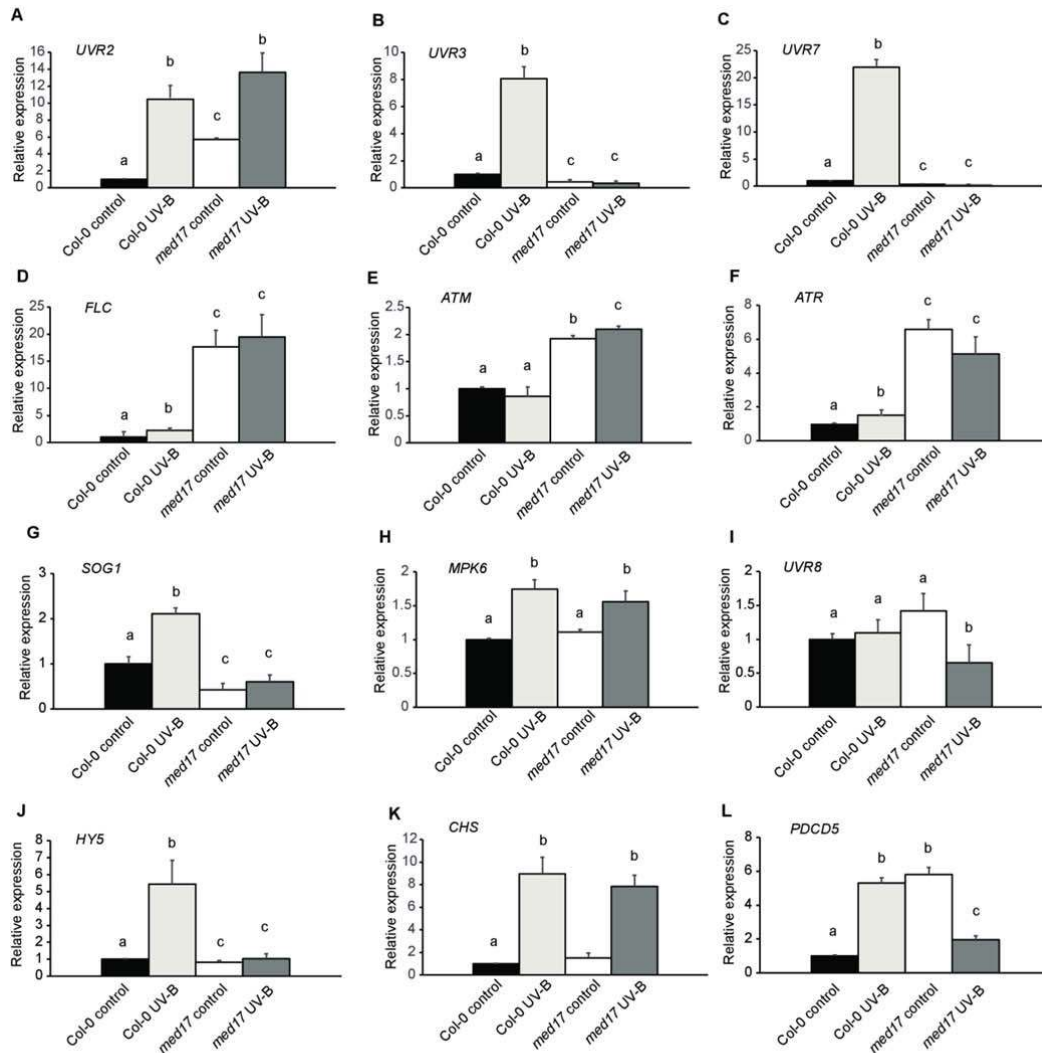


**Figure 4** UV-B effect on expression of genes that participate in UV-B responses in WT Col-0 and *med17* seedlings. Relative expression levels of *UVR2* (A), *UVR3* (B), *UVR7* (C), *FLC* (D), *ATM* (E), *ATR* (F), *SOG1* (G), *MAPK6* (H), *UVR8* (I), *HY5* (J), *CHS* (K) and *PDCD5* (L) analyzed by RT-qPCR in WT Col-0 and *med17* seedlings under control conditions or immediately after a 4 h-UV-B treatment (UV-B). Results represent the average  $\pm$  SEM. Different letters indicate statistically significant differences applying an ANOVA test ( $P < 0.05$ ). Data represent at least three biological replicate experiments. Each RT-qPCR was repeated at least three times on each biological replicate.

312 (Figure 4, I), was similarly expressed in *med17* and WT seedlings under control  
 313 conditions, but showed a small but significant repression after UV-B exposure in the  
 314 mutant. *HY5*, which encodes a transcription factor that regulates UV-B responses in the  
 315 *UVR8* pathway and showed decreased expression in *med17* plants in the RNA seq data  
 316 (Supplemental Table S1), also showed decreased levels after UV-B exposure (Figure 5,  
 317 J). Thus, under UV-B conditions, *med17* mutants have decreased expression of  
 318 important regulators of the UV-B photomorphogenic pathway. Finally, *CHALCONE*  
 319 *SYNTHASE* (*CHS*) transcript levels in *med17* were analyzed. *CHS* is a target of *HY5*

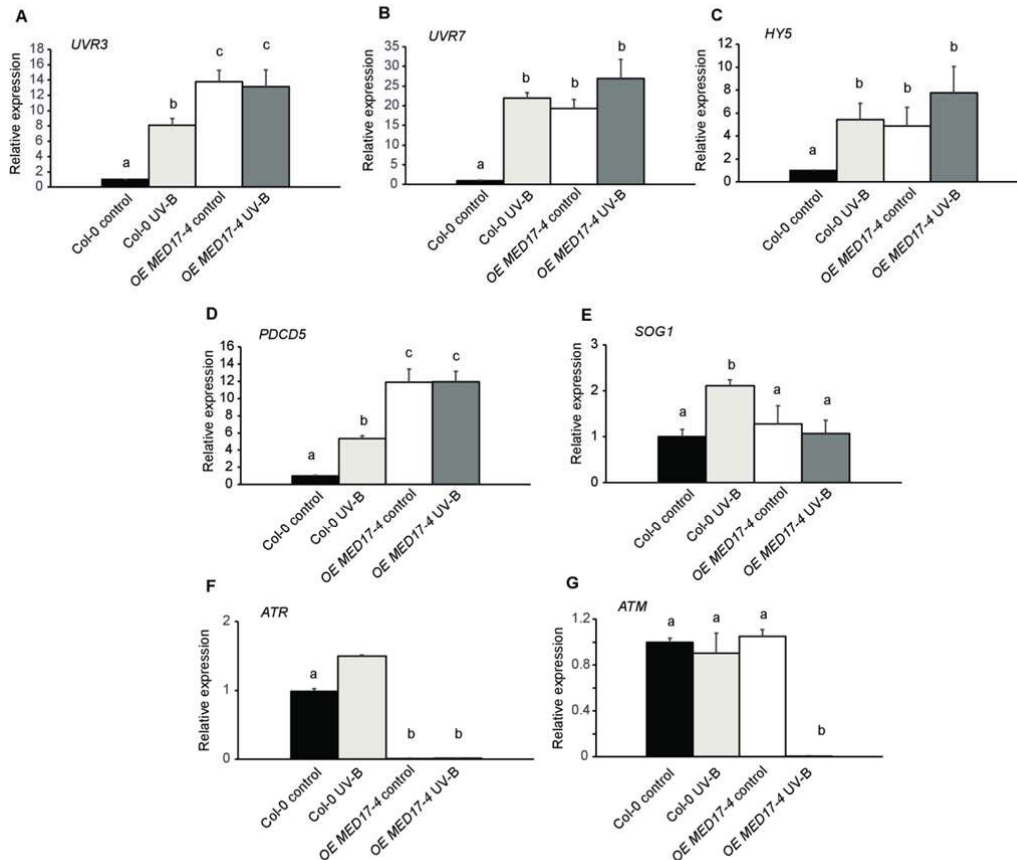


**Figure 5** UV-B effect on expression of genes that participate in UV-B responses in WT Col-0 and OE MED17 seedlings. Relative expression levels of *UVR3* (A), *UVR7* (B), *HY5* (C), *PDCD5* (D), *SOG1* (E), *ATR* (F) and *ATM* (G) analyzed by RT-qPCR in WT Col-0 and OE MED17-4 seedlings under control conditions or immediately after a 4 h-UV-B treatment (UV-B). Results represent the average  $\pm$  SEM. Different letters indicate statistically significant differences applying an ANOVA test ( $P < 0.05$ ). Data represent at least three biological replicate experiments. Each RT-qPCR was repeated at least three times on each biological replicate.

320 and encodes the first enzyme in the flavonoid pathway; these specialized metabolites  
 321 provide UV-B protection in plants (Falcone Ferreyra et al., 2012). *CHS* expression was  
 322 not altered in *med17* mutants, neither under control conditions nor after exposure  
 323 (Figure 4, K). Interestingly, other transcripts that encode enzymes in the flavonoid  
 324 pathway, such as *FLAVONOL SYNTHASE 1*, *CHALCONE ISOMERASE 1 and 3*,  
 325 *FLAVONOID 3'-MONOOXYGENASE (CYP75B1)*; and the transcription factor *MYB*  
 326 *111*, which regulates the expression of enzymes in the flavonoid pathway, belong to  
 327 cluster 1 in the RNAseq data (Figure 1, B, Supplemental Table S1). These transcripts  
 328 show decreased expression in *med17* mutants under control conditions. Despite this,  
 329 flavonoid levels in *med17* and OE MED17 plants were similar to those in WT plants  
 330 (Supplemental Figure S2, D), correlating with the expression patterns of *CHS*. In this  
 331 way, increased sensitivity to UV-B in *med17* plants is not due to changes in flavonoid  
 332 accumulation.



333 On the other hand, when transcript levels of DNA repair enzymes with altered  
334 expression in *med17* mutants were analyzed in *OE MED17* plants, results showed that  
335 *UVR3* and *UVR7* were highly expressed in the transgenic plants, both under control  
336 conditions and after UV-B exposure (Figure 5, A, B), suggesting that lower CPD levels  
337 in *OE MED17* plants after UV-B exposure are due to high expression of these DNA  
338 repair enzymes. Interestingly, UV-B up-regulation of both genes is lost in the *OE*  
339 *MED17* plants; and this is also true for other UV-B responsive genes such as *HY5* and  
340 *SOG1* (Figure 5, C-E). Therefore, MED17 could mediate UV-B regulation of at least  
341 some UV-B marker genes, this may be through its regulation of *HY5* expression. On the  
342 contrary, both *ATR* and *ATM*, which were expressed at high levels in *med17* mutants,  
343 showed very low levels in *OE MED17* plants, in particular after UV-B exposure (Figure  
344 5, F, G); thus, MED17 is a negative regulator of both DDR kinases.

345 Together, qRT-PCR results demonstrate that, for at least some genes, in  
346 particular *HY5*, *UVR3*, and *UVR7*, the upregulation after UV-B is lost in *med17* and  
347 constitutively increased in *OE MED17* seedlings; therefore, at least some of the  
348 phenotypes observed in UV-B irradiated plants could be due to altered expression these  
349 genes.

350

351 MED17 interacts with nuclear proteins with roles during DNA repair

352

353 As described in the Introduction, in humans and yeasts, MED17, besides being a  
354 transcriptional regulator, also physically interacts with proteins that participate in DNA  
355 repair through the NER system. Therefore, to analyze if in Arabidopsis there is also a  
356 physical interaction of MED17 with DNA repair enzymes after UV-B exposure,  
357 Arabidopsis nuclei were obtained from UV-B irradiated *med17* mutants expressing  
358 *MED17* fused to *GFP* under the *35S* promoter. Expression of this fusion protein  
359 complemented the mutant phenotypes suggesting it is active *in vivo* (Supplemental  
360 Figure S3).

361 MED17 was co-immunoprecipitated from purified nuclei using anti-GFP  
362 antibodies, and the output was analyzed by LC-MS/MS (Smaczniak et al., 2012). Sixty-  
363 five nuclear proteins coimmunoprecipitated with MED17-GFP in at least 2 of 3  
364 biological replicates from UV-B treated plants (Supplemental Table S3). In this group,  
365 there were other Mediator proteins, such as MED8, MED37 A/B, C and F; transcription  
366 initiation and splicing factors, chromatin associated proteins and other transcription

367 factors (Supplemental Table S3). Interestingly, several proteins which were previously  
368 described to have a role during DNA repair were identified, such as the cohesin factor  
369 PDS5C (Pradillo et al., 2015), the histone chaperones NAP 1; 3 and NRP 1 and 2  
370 (Casati and Gomez, 2021), two DEK domain-containing chromatin associated proteins  
371 (Waidmann et al., 2014), a sister chromatid cohesion 1 protein 4 (SYN4; da Costa-  
372 Nunes et al., 2004); a DNA repair ATPase-related protein and a replication factor C  
373 subunit 4 (Chen et al., 2018; Table 1, Supplemental Table S3). LC-MS data showed that  
374 MED17 is in a same complex with the transcription initiation factor TFIID subunit 9  
375 and the transcription initiation factor IIE subunit alpha; therefore, MED17, together  
376 with these proteins, may be required for correct TCR repair as previously described in  
377 other species. Moreover, a cell division cycle 5-like protein (CDC5) was also found to  
378 immunoprecipitate with MED17 in plants exposed to UV-B, this protein has a role in  
379 cell cycle control and also in the response to DNA damage (Table 1; Lin et al., 2007).  
380 Thus, MED17 may not only directly participate in DNA repair, but it may also regulate  
381 the DNA damage response by interacting with other proteins acting downstream in the  
382 DDR pathway. This data suggests that, as demonstrated in yeasts and humans,  
383 AtMED17, besides having a role in transcription regulation by UV-B as shown in  
384 Figures 4 and 5, it could have a direct role interacting with nuclear proteins during DNA  
385 repair.

386

387 *atr* mutant phenotypes are suppressed in the absence of MED17

388

389 To further analyze the role of MED17 in the DDR, we crossed *med17* mutants with  
390 either *atm* or *atr* plants to generate the corresponding double mutants. Ataxia  
391 telangiectasia mutated (ATM) is usually activated by double-strand breaks in the DNA;  
392 while ATR is mainly triggered by single-strand breaks or stalled replication forks such  
393 as CPDs and 6-4PPs that occur after UV-B exposure; and both independently regulate  
394 the DNA damage response in plants (Culligan et al., 2006). For the *med17 atm* crosses,  
395 only heterozygous mutants in either or both genes were obtained after screening 60  
396 plants, but no double homozygous mutant plants were recovered, suggesting that *med17*  
397 deficiency generates lesions that require ATM to allow cell viability. On the contrary,  
398 *med17 atr* double homozygous mutants were obtained (Supplemental Figure S6).  
399 *med17 atr* plants were smaller than WT and *atr* plants when grown under standard  
400 growth conditions in the growth chamber, but they looked like *med17* mutants

401 (Supplemental Figure S6, A). As *med17* single mutants, the double mutants had smaller  
402 leaves than WT and *atr* plants (Supplemental Figure S6, A). In addition, both the single  
403 *med17* and double *med17 atr* mutants displayed a significant reduction in the siliques  
404 length compared to WT and *atr* plants (Supplemental Figure S6, B and C). The number  
405 of seeds per silique in *med17* and *med17 atr* mutants was also decreased compared to  
406 WT and *atr* (Supplemental Figure S6, D). When the seeds in each silique were  
407 observed, *med17* and *med17 atr* mutants showed both fertilized seeds and aborted  
408 embryos, which correlates with the failure observed in seed production (Supplemental  
409 Figure S6, B, E and F). In contrast, both WT and *atr* mutants showed low and similar  
410 number of aborted seeds (Supplemental Figure S6, E and F). In order to analyze if  
411 embryos had dead cells, seeds were stained with propidium iodide and analyzed by  
412 confocal microscopy (Supplemental Figure S7). While WT and *atr* seeds showed a very  
413 low number of stained cells, both *med17* and *med17 atr* seeds showed higher staining.  
414 These results could explain the decreased fertility observed in *med17* and *med17 atr*  
415 mutants.

416 When plants were exposed to UV-B radiation, all mutants accumulated similar  
417 levels of CPDs and higher than those in WT plants (Figure 6, A). On the other hand,  
418 PCD was analyzed in the meristematic zone of the primary roots one day after a UV-B  
419 treatment and *med17 atr* mutants showed significantly fewer dead cells than *atr* and WT  
420 plants (Supplemental Figure S8). Moreover, 4 days after the treatment, *atr* mutants still  
421 had higher number of dead cells than the other lines under study, while *med17* and  
422 *med17 atr* mutants had a similar number of dead cells and higher than those in WT  
423 plants, which were almost recovered (Figure 6, B and C).

424 The effect of UV-B was investigated on the meristematic zone of the primary  
425 roots. The size of the meristematic zone of the primary roots from *atr* seedlings was  
426 similar to that of WT primary roots under control conditions in the absence of UV-B,  
427 while the size of that in the double mutant was significantly smaller (Figure 7a). In UV-  
428 B treated roots, there was a significant decrease in the meristematic zone size in all  
429 lines; however, the decrease observed was significantly higher in *atr* mutants, while  
430 *med17 atr* plants showed a similar decrease as that in *med17* plants (Figure 7, A and B).  
431 This higher decrease in the meristem size in *atr* plants was a consequence of a higher  
432 decrease in the cortex cell number in the root meristem than that in *med17*, *med17 atr*  
433 and WT plants by UV-B, while all lines showed a similar increase in the cell area after  
434 the treatment (Figure 7, C-F). Similarly as for all other parameters analyzed, MED17 is

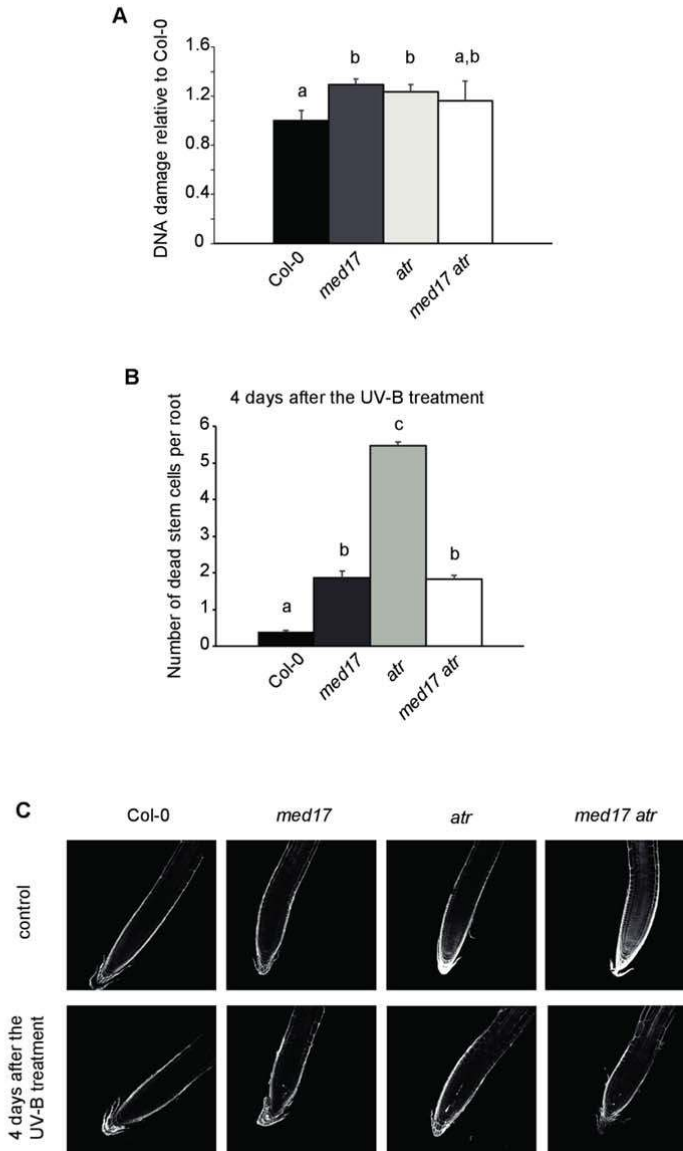


**Figure 6** Characterization of DNA damage responses in double *med17 atr* mutant plants. A, Relative CPD levels in the DNA of WT Col-0, *med17*, *atr* and *med17 atr* plants immediately after a 4-h UV-B treatment under light conditions. Results represent averages  $\pm$  S.E.M. of six independent biological replicates. B, Programmed cell death in meristematic root cells in Col-0, *med17*, *atr* and *med17 atr* plants 4 days after UV-B exposure. Results represent the average of at least 50 biological replicates  $\pm$  S.E.M. Different letters indicate statistically significant differences applying analysis of variance test ( $p < 0.05$ ). C, Representative images of stem cells and adjacent daughter cells from WT Col-0, *med17*, *atr* and *med17 atr* seedlings that were scored for intense PI staining

435 required for the higher inhibition of cell proliferation in the meristematic zone of the  
436 primary roots observed in *atr* mutants under UV-B conditions. Therefore, *atr*  
437 phenotypes are suppressed in the absence of MED17. Interestingly, *med17* seedlings  
438 show increased *ATR* expression (Fig 6f); thus, the similar phenotypes observed in  
439 *med17* and *med17 atr* double mutants are independent of *ATR* levels.

440

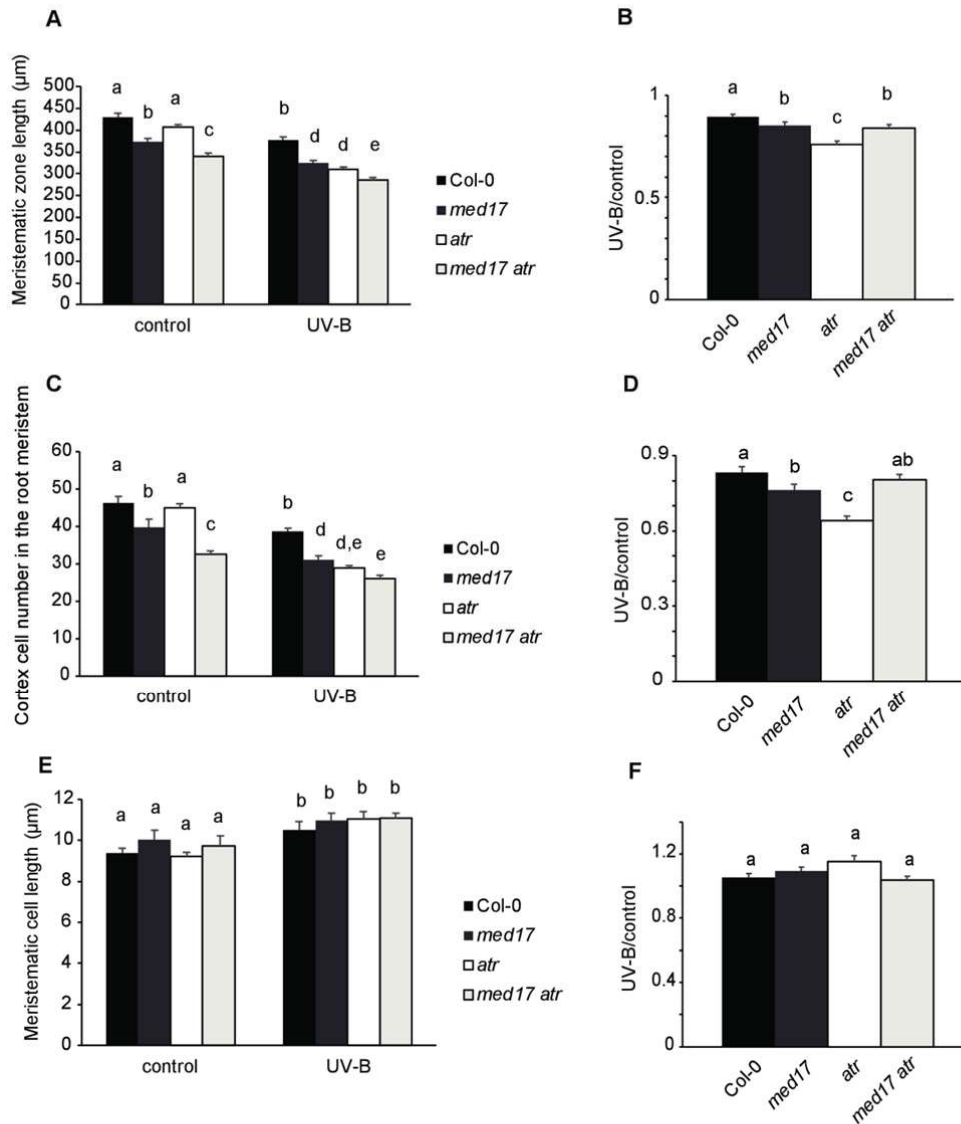


**Figure 7** UV-B root meristematic zone of *med17 atr* is similarly affected by UV-B as *med17* seedlings but differently than *atr* mutants. A, Average of meristematic root zone length; C, cortex cell number; E, cortex cell length in the root meristem from WT Col-0, *med17*, *atr* and *med17 atr* seedlings after 4 days of a UV-B treatment or under control condition. B, D and F, Ratio between meristematic root zone length (B), cortex cell number (D), and cortex cell area values (F) measured after UV-B exposure vs those under control conditions are shown. Results represent the average  $\pm$  S.E.M. Different letters indicate statistically significant differences applying analysis of variance test ( $P < 0.05$ ).

441 MED17 deficiency is overcome by PDCD5 overexpression during DNA damage  
 442 conditions after UV-B exposure

443

444 In addition, we investigated whether the role of MED17 in the DDR after UV-B  
 445 exposure was affected in plants with altered expression of *PDCD5*. Previously, we  
 446 showed that AtPDCD5 participates in the DNA damage response after UV-B exposure

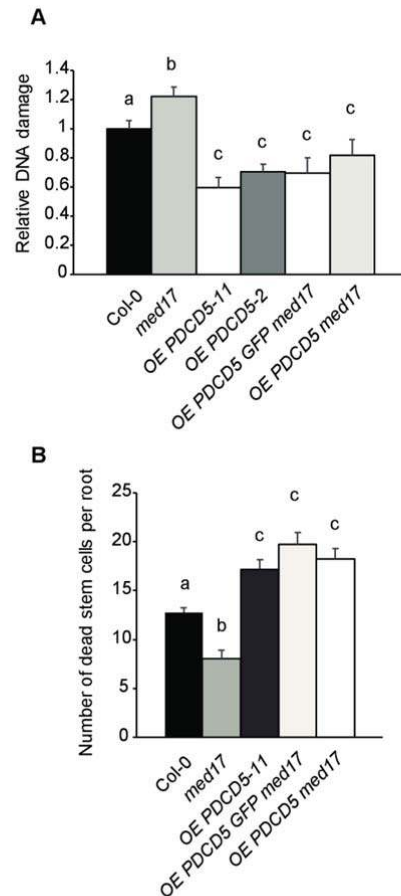


**Figure 8** Characterization of DNA damage responses in *OE PDCD5 med17* plants. A, Relative CPD levels in the DNA of WT Col-0, *med17*, *OE PDCD5* and *OE PDCD5 med17* plants immediately after a 4-h UV-B treatment under light conditions. Results represent averages  $\pm$  S.E.M. of six independent biological replicates. B, Programmed cell death in meristematic root cells of WT Col-0, *med17*, *OE PDCD5* and *OE PDCD5 med17* plants 1 day after UV-B exposure. Results represent the average of at least 50 biological replicates  $\pm$  S.E.M. Different letters indicate statistically significant differences applying analysis of variance test ( $P < 0.05$ ).

447 in Arabidopsis (Falcone Ferreyra et al., 2016). Plants that overexpressed AtPDCD5  
448 accumulated lower levels of DNA damage after UV-B exposure and showed more PCD  
449 in root tips upon UV-B exposure (Falcone Ferreyra et al., 2016). Thus, we obtained  
450 transgenic plants that overexpressed PDCD5 in a *med17* mutant background by genetic  
451 crosses. When we analyzed DNA damage accumulation after UV-B in these plants, they  
452 showed lower amounts of CPDs than *med17* mutants, and even lower than WT plants,  
453 with CPD levels similar to those measured in *OE PDCD5* lines in a WT background  
454 (Figure 8, A). Moreover, when PCD was analyzed in the *OE PDCD5 med17* line one  
455 day after a UV-B treatment, these transgenic plants had a higher number of dead cells in  
456 the meristematic root zone than WT and *med17* roots, and similar to *OE PDCD5* plants

457 in a WT background (Figure 8, B). Thus, after UV-B exposure, *PDCD5* overexpression  
458 counteracts the deficiency of *MED17* during the DDR.

459 When the expression of *PDCD5* was analyzed in *med17* and *OE MED17*  
460 seedlings, transcripts were significantly lower in *med17* than in WT after UV-B  
461 exposure, despite the opposite was observed under control conditions (Figure 4, L);  
462 while in *OE MED17* plants *PDCD5* expression was significantly higher than in WT  
463 plants, both under control conditions and after UV-B exposure (Figure 5, D). In this  
464 way, some of the phenotypes of *med17* and *OE MED17* plants after UV-B could be the  
465 result of altered *PDCD5* expression.

466

467

468 **Discussion**

469

470 MED17 is a subunit of the head module of the Mediator complex, it has an important  
471 role interacting with several other Mediator subunits, being a key scaffold component of  
472 the whole complex (Guglielmi et al., 2004; Cevher et al., 2014; Maji et al., 2019). In  
473 Arabidopsis, MED17 is required for smRNA biogenesis and for the repression of  
474 heterochromatic loci, suggesting that this Mediator subunit, besides having a role in  
475 transcription, it would also participate in genome stability (Kim et al., 2011). In this  
476 work, we aimed to investigate the role of AtMED17 in UV-B responses. The analysis of  
477 the transcriptome profile of *med17* mutants compared to that of WT plants grown under  
478 white light conditions showed that of the 6822 genes that showed altered expression in  
479 *med17* mutants, 32% were also UV-B regulated in WT Col-0 plants reported in  
480 previous experiments (Tavridou et al., 2020). Of these 2184 genes, about 56% showed  
481 low expression in *med17* mutants and were up-regulated by UV-B in WT plants,  
482 suggesting that MED17 has a positive role in the regulation of UV-B responsive genes  
483 in Arabidopsis plants. In this group and as shown in Supplemental Figure S1, C, we  
484 found *RUP1* and *RUP2*, which encode two highly related WD40-repeat proteins that are  
485 negative regulators of the UVR8 photoreceptor in UV-B photomorphogenic responses  
486 (Gruber et al., 2010). *HY5* and *HYH*, which encode transcription factors that mediate  
487 UV-B responses of the UVR8-dependent pathway and activate the expression of *RUP1*  
488 and *RUP2*, also showed decreased expression in *med17* mutants. *CRY1* and *CRY3*,  
489 which are blue light photoreceptors in the nuclei (*CRY1*) and in the chloroplasts and  
490 mitochondria (*CRY3*; Liu et al., 2011), were also down-regulated in *med17* plants. In  
491 particular, *CRY3* belongs to the CRY-DASH clade of the photolyase/cryptochrome  
492 superfamily, and besides acting as a photoreceptor, it may also have single-strand DNA  
493 repair activity (Selby and Sancar, 2006; Pokorny et al., 2008). Interestingly, *UVR3*,  
494 which encodes an enzyme with 6–4 photolyase activity in Arabidopsis (Nakajima *et al.*,  
495 1998), increased in response to UV-B in WT, but not in *med17* plants, and was  
496 constitutively highly expressed in *OE MED17* plants. On the other hand, other genes  
497 that encode DNA recombination and repair, such as *RADA* and *RAD23 B-D* (Ishibashi  
498 et al., 2006; Lahari et al., 2018) showed up-regulation in *MED17* deficient plants,  
499 demonstrating that MED17 is required for proper expression of DNA repair enzymes.

500 In yeast, MED17 physically interacts with Rad2/XPG and participates in DNA  
501 repair after UV exposure, recruiting Rad2 to transcribed genes (Eyboulet et al., 2013).



502 Moreover, in human cells, MED17 interacts with a DNA helicase XPB subunit of  
503 TFIIH, which is essential for both transcription and NER, and similarly as it was  
504 described in yeast, MED17 plays an important role switching between transcription and  
505 DNA repair (Kikuchi et al., 2015). After immunoprecipitation studies using transgenic  
506 plants expressing *MED17-GFP*, we demonstrated that in Arabidopsis, MED17 also  
507 directly or indirectly interacts with proteins that participate in DNA repair, such as the  
508 histone chaperones NAP 1; 3 and NRP 1 and 2 (Casati and Gomez, 2021) and a DNA  
509 repair ATPase-related protein and a replication factor C subunit 4 (Chen et al., 2018).  
510 Moreover, the results presented here show that *med17* mutants accumulate higher DNA  
511 damage than WT plants, while plants that overexpress *MED17* accumulate lower  
512 amounts of CDPs after UV-B exposure. In this way, and similarly as MED17 from  
513 yeast and humans, AtMED17 has a role in DNA repair. In yeast and humans, MED17  
514 participates in transcription-coupled DNA repair (TCR) by NER DNA repair pathway,  
515 which removes DNA lesions that interfere with the progression of the RNA polymerase  
516 through transcribed genes (Eyboulet et al., 2013; Kikuchi et al., 2015; Hanawalt and  
517 Spivak, 2008). In Arabidopsis, *med17* plants are deficient not only in dark repair, which  
518 in plants is mostly achieved by NER, but also during light conditions, mostly  
519 accomplished by photolyases (Spampinato, 2017). Our results show that AtMED17  
520 associates in a same complex with the transcription initiation factors TFIID subunit 9  
521 and TFIIE subunit alpha, which may participate in TCR repair. Additionally, MED17,  
522 directly or indirectly interacting with the Replication Factor C subunit 4, could have a  
523 role in DNA repair by the NER system in Arabidopsis. AtMED17 also co-  
524 immunoprecipitated with histone chaperones and other chromatin associated factors,  
525 which may be required for proper dark DNA repair but also during photoreactivation.  
526 Thus, *med17* plants may be deficient in DNA repair due to decreased TCR repair and  
527 because MED17 may be necessary to interact with chromatin proteins during DNA  
528 repair. In addition, *med17* plants may accumulate more DNA damage after UV-B  
529 exposure because they express lower levels of some photolyases and other DNA repair  
530 proteins.

531 In addition, *med17* mutants showed a higher inhibition of cell proliferation in the  
532 root meristems after a UV-B treatment, and the meristems had less dead cells 1 day  
533 after, while they still presented dead cells after 4 days, in contrast to WT primary roots  
534 which showed more dead cells 1 day after the treatment but completely recovered after  
535 4 days. These results suggest that MED17 may also participate in other aspects of the

536 DDR besides DNA repair. A low accumulation of dead cells persisting after exposure  
537 under genotoxic conditions was also previously observed in *sog1* mutants (Johnson et  
538 al., 2018). SOG1 is a transcription factor that, in *Arabidopsis thaliana*, is a master  
539 regulator of genes that participate in the DNA damage response, including in the  
540 activation of programmed cell death in the meristematic cells in the roots. Johnson et al.  
541 (2018) demonstrated that, in contrast to WT plants, *sog1* mutants are defective in  
542 damage-induced programmed cell death and fail to undergo cell division in the primary  
543 roots meristems. A similar response was also observed in *med17* mutants in our  
544 experiments. Interestingly, *SOG1* transcript levels were significantly decreased in  
545 *med17* plants, suggesting that the PCD phenotype and the inhibition of cell proliferation  
546 in the primary root meristems after UV-B exposure in the *MED17* deficient plants can  
547 be due to decreased expression of this transcription factor.

548 Interestingly, other Mediator subunits have been shown to participate in PCD  
549 and root development, for example MED18, which is also a subunit of the Mediator  
550 head. *med18* mutants show a reduction in primary root growth, with an increase in  
551 lateral root formation and root hair development (Raya-Gonzalez et al., 2018). *med18*  
552 roots had altered cell division and elongation with an increased auxin response and  
553 transport at the root tip. Moreover, *med18* seedlings showed PCD in the root meristem  
554 in the absence of any genotoxic stress, which increased with age and/or exposition to  
555 DNA-damaging agents (Raya-Gonzalez et al., 2018). Despite MED17 and MED18 are  
556 both components of the Mediator head, they have different roles at least during DNA  
557 damage conditions. For example, while *med18* roots show high PDC in the  
558 meristematic primary root zone even in the absence of any genotoxic agent; *med17*  
559 roots show an opposite phenotype, with very low number of dead cells after UV-B  
560 exposure, and undetectable dead cells under control conditions in the absence of UV-B.  
561 Moreover, while meristematic cells in the primary roots of *med18* seedlings are bigger  
562 than those in WT roots (Raya-Gonzalez et al., 2018); cells in the meristematic zone of  
563 *med17* plants are similar to those in WT plants. *med17* root meristems are shorter than  
564 WT root meristems because they have less cells, and they show a higher decrease in the  
565 number of cells after UV-B exposure, suggesting that while MED18 may have an  
566 important role controlling cell size, MED17 may mostly control cell proliferation.

567 In *Arabidopsis*, both ATR and/or ATM regulate DNA damage responses after  
568 UV-B exposure (Furukawa et al., 2010). The double *med17 atr* mutant showed similar  
569 phenotypes as those of *med17* mutants, both under control conditions and after UV-B

570 exposure; thus, MED17 is required for a proper activation of the DNA response  
571 mediated by ATR. It is possible that MED17 could act upstream ATR, for example  
572 interacting with DNA repair proteins during DNA damage recognition. The absence of  
573 proper damage recognition due to MED17 deficiency may therefore affect the activation  
574 of the DDR through ATR. However, we cannot rule out that MED17 may modulate  
575 ATR activity in other ways, for instance regulating the expression of proteins required  
576 for ATR activation of the DDR.

577 We previously characterized a UV-B inducible protein, AtPDCD5, which is  
578 similar to human PDCD5, a PCD-associated protein (Falcone Ferreyra et al., 2016; Xu  
579 et al., 2009). In humans, PDCD5 interacts with a histone acetyltransferase of the MYST  
580 family, TIP60, which are together recruited to chromatin in response to DNA damage,  
581 where they participate in different stages of repair (Murr et al., 2006; Xu et al., 2009).  
582 On the other hand, PDCD5 is also involved in the activation of PCD in the cytosol  
583 (Zhuge et al., 2011). *pdcd5* mutants accumulate higher levels of CPDs than WT plants  
584 after UV-B exposure but lower PCD in the primary root tip; these phenotypes are  
585 similar to those of *med17* mutants. On the contrary, plants overexpressing *AtPDCD5*  
586 were less sensitive to DNA damage and showed more dead cells in the root meristems  
587 after UV-B exposure (Falcone Ferreyra et al., 2016). Our results show that  
588 overexpression of *PDCD5* counteracts the deficiency in MED17 levels. As *PDCD5*  
589 levels are affected in plants with altered *MED17* expression, some of the phenotypes  
590 after UV-B exposure in *med17* and *OE MED17* plants could be, at least in part, the  
591 result of altered *PDCD5* expression.

592 In summary, our results demonstrate that MED17 regulates different plant  
593 responses to UV-B in Arabidopsis plants, in particular the DDR. According to the  
594 presented data, MED17 not only transcriptionally modulates the expression of genes of  
595 the DDR and the UV-B pathway, but it also physically interacts with transcription  
596 initiation factors and/or chromatin proteins that could facilitate DNA repair. Finally, we  
597 here show that MED17 is required for the *atr* mutant phenotypes, and that its deficiency  
598 is overcome by *PDCD5* overexpression. The interaction of MED17 with ATR and  
599 PDCD5 during the DDR may be regulating gene expression of proteins in the pathway,  
600 but it may also be during the early recognition of DNA damage through the binding  
601 with DNA repair proteins, which may be necessary for the activation of the pathway.

602

603 **Materials and methods**

604

605 Plant material, growth conditions and UV-B treatments

606

607 *A. thaliana* ecotype Col-0 was used for all experiments. *med17-1* (SALK\_102813)  
608 mutants were provided by Dr. Xuemei Chen (University of California, Riverside, USA).  
609 *atr-2* (SALK\_03284) and *atm-2* (SALK\_006953) seeds were provided by Dr. Roman  
610 Ulm (University of Geneva, Switzerland). *OE PDCD5* transgenic plants (Falcone  
611 Ferreyra et al., 2016), *atr-2* or *atm-2* single mutants were crossed with *med17* mutants  
612 and the F2 population was screened by PCR using specific primers for *MED17*, *ATR*,  
613 *ATM* and *PDCD5* genes (Supplemental Table S4). For all experiments, F3 plants were  
614 used.

615 Arabidopsis plants were sown on soil, stratified for 3 days at 4 °C and they were  
616 then moved to a growth chamber. Plants were grown at 22 °C under a 16-h-light/8-h-  
617 dark photoperiod (100  $\mu\text{E m}^{-2}\text{s}^{-1}$ ). For root and hypocotyl studies, plants were  
618 germinated and grown on petri plates containing Murashige and Skoog salt (MS)-agar  
619 (0.7 % w/v) medium for 5 days.

620 For all UV-B treatments except for flowering time assays, plants were irradiated  
621 with UV-B lamps using fixtures mounted 30 cm above the plants (2  $\text{W m}^{-2}$  UV-B and  
622 0.6  $\text{W m}^{-2}$  UV-A, Bio-Rad ChemiDoc™XRS UV-B lamps, catalogue 1708097). The  
623 lamps have emission spectra from 290 to 310 nm, with a maximum emission peak at  
624 302 nm. The bulbs were covered using cellulose acetate filters (100 mm extra-clear  
625 cellulose acetate plastic, Tap Plastics, Mountain View, CA); the cellulose acetate filters  
626 absorb wavelengths lower than 290 nm without removing UV-B from longer  
627 wavelengths. As a control treatment without UV-B, plants were exposed for the same  
628 period of time under lamps covered with a polyester plastic that absorbs UV-B at  
629 wavelengths lower than 320 nm. For root and hypocotyl elongation assays, seedlings  
630 were irradiated for 1 h. For DNA damage analysis, 4-week-old plants were irradiated  
631 with UV-B for 4 h, and leaves were collected immediately and after 2 h of recovery in  
632 the absence of UV-B, either under light or dark conditions. UV radiation was measured  
633 using a UV-B/UV-A radiometer (UV203 AB radiometer; Macam Photometrics).

634 For flowering time analysis, white light was supplemented with 2  $\text{W m}^{-2}$  of UV-  
635 B (311 nm; Phillips narrowband TL/01 lamps) during 1 h every day starting from day 9  
636 after transferring to the growth chamber until flowering, the zeitgeber time of UV-B  
637 treatments was 4 h in long day conditions.

638 For seedling lethality analysis, seeds were sown in agar plates and stratified for 3  
639 days. Then, they were irradiated with white light ( $100 \mu\text{E m}^{-2} \text{s}^{-1}$ ) for 1 h and, after that,  
640 they were kept 24 h in the dark. Next, plates were treated with UV-B for 1 h, transferred  
641 to darkness for 48 h and then they were finally allowed to grow in the growth chamber  
642 for 15 days under normal light conditions (UV-B irradiated plants). Alternatively, a  
643 different group of seedlings were grown under the same conditions but they were not  
644 UV-B irradiated (darkness treated plants). Additionally, seedlings were stratified for 3  
645 days and they there were grown under normal growth conditions for 18 days (light  
646 grown plants).

647 UV radiation was measured using a UV-B/UV-A radiometer (UV203 AB  
648 radiometer; Macam Photometrics).

649

650 DNA damage analysis

651

652 12 DAS leaf samples from plants treated with UV-B or kept under control conditions  
653 were collected immediately or 2 hours after the end of the treatment and immersed in  
654 liquid nitrogen. CPD accumulation in the DNA purified from the collected samples was  
655 analyzed as described previously (Lario et al., 2013). UV-B treatments were performed  
656 both under light and dark conditions; plants irradiated under dark conditions were  
657 allowed to recover for 2 h under light or dark conditions. 0.1 g were collected and  
658 extracted DNA was dot blotted onto a nylon membrane (Perkin-Elmer Life Sciences).  
659 The blot was incubated with monoclonal antibodies specific to CPDs (TDM-2) from  
660 Cosmo BioCo (1:2,000 in TBS). Quantification was achieved by densitometry of the  
661 dot blot using Image-Quant software version 5.2.

662

663

664 Root meristem analysis and programmed cell death after UV-B exposure

665

666 Seedlings were grown for 5 days in vertically oriented Murashige and Skoog plates, and  
667 were then irradiated with UV-B light or kept without UV-B. UV-B-irradiated and  
668 control seedlings were then incubated for 24 hr or 96 hr in the growth chamber, and  
669 then PCD was analyzed as described by Furukawa et al. (2010). Root tips were stained  
670 using a modified pseudo-Schiff propidium iodide staining protocol and visualized by  
671 confocal laser scanning microscopy (Nikon C1) under water with a 40× objective. The

672 excitation wavelength for propidium iodide-stained samples was 488 nm, and emission  
673 was collected at 520 to 720 nm. Dead (intensely Propidium iodide (PI)-staining) cells in  
674 the vicinity of the quiescent centre were counted and scored as dead cells per root.

675

#### 676 Generation of Arabidopsis transgenic plants

677

678 cDNA was obtained from leaf tissues of WT plants grown under continuous light  
679 growth. *MED17* cDNA without its stop codon was amplified using specific primers  
680 including *KpnI* and *XhoI* restriction sites (Table S1). PCR was done using Pfu  
681 (Invitrogen) polymerase under the following conditions: 94°C for 5 min; 40 cycles of  
682 94°C for 30 sec, 55°C for 20 sec and 72°C for 30 sec; and finally, one cycle at 70°C for  
683 2 min. PCR product was purified from the gel, cloned in a pBluescript vector and  
684 sequenced. The construct was then transformed into *E. coli* DH5 $\alpha$  and then the plasmid  
685 was purified and digested with *KpnI* and *XhoI*. The digestion fragment corresponding to  
686 *MED17* was subcloned into the pCardo plasmid, and the construct expressing *MED17*  
687 under the *35S* promoter was transformed into *Agrobacterium tumefaciens* strain  
688 GV3101. Col 0 was transformed using the floral dip method (Clough and Bent, 1998). In  
689 addition, the pBluescript vector with *MED17* cDNA was digested using *Kpn* and *Sall*  
690 and the fragment was cloned into pCS052\_GFP\_pCHF3 (a modified version of pCHF3;  
691 with the GFP coding sequence without the start codon inserted into *Sall*-*PstI* sites). The  
692 resulting construct, pCHF3:*MED17*-GFP, was transformed into *E. coli* DH5 $\alpha$  and  
693 purified. The construct was transformed into *Agrobacterium tumefaciens* GV3101 and  
694 Col 0 and *med17* plants were transformed using the floral dip method. Transformed  
695 seed (T1) were identified by selection on solid MS medium containing kanamycin (30  
696 mg L<sup>-1</sup>, pCHF3) or BASTA (3 mg mL<sup>-1</sup>, pCardo, and finally plants were transferred to  
697 soil. The presence of *Pro35S:MED17* (*OE MED17*) and *Pro35S:MED17-GFP* (*OE*  
698 *MED17-GFP*) transgenes in T2 plants was screened by PCR using genomic DNA  
699 (Table S1).

700

#### 701 Flowering time analysis

702

703 Flowering time was determined by counting the number of rosette leaves or the number  
704 of days until the first flower opens, similar to previous reports (Dotto et al., 2018).

705 Flowering time was counted as the number of rosette leaves at the moment of flowering  
706 or the number of days until the first flower opens.

707

708 Seed analysis

709

710 Seeds were phenotypically analyzed using a Nikon SMZ-10 microscope. For silique  
711 analyzes, 56 siliques from each genotype were analyzed, and the number of aborted  
712 seeds per silique were counted. After that, seeds were stained using PI stain and they  
713 were then observed using confocal laser scanning microscopy, using a Confocal Nikon  
714 C1 microscope.

715

716 RNA-seq experiments

717 For the RNA-seq experiments, WT and *med17* seeds were sown on MS medium with  
718 0.8 % (w/v) agar, kept at 4°C for three days and then grown for 10 days at 23°C under  
719 long day (16 h light, 8 h dark, 100  $\mu\text{E m}^{-2} \text{s}^{-1}$ ) of white fluorescent light. Three  
720 independent biological replicates for each genotype were harvested 2 h before the start  
721 of the night period and the seedlings were immediately frozen in liquid nitrogen. Total  
722 RNA was prepared using a Plant Total RNA Mini Kit (YRP50).

723 FASTQC v0.11.5 was used for quality control of the FASTQ sequence files  
724 (Andrews, 2010). Illumina 150-bp paired-end reads were mapped to the *A. thaliana*  
725 reference genome assembly (assembly version TAIR10) with HISAT2 (Kim et al.,  
726 2015) and raw read counts per gene were then estimated with htseq-count (Anders et al.,  
727 2015) and normalized according to trimmed mean of M-values (TMM) (Robinson and  
728 Oshlack, 2010). Over 22 million reads were obtained for each sample, with an overall  
729 alignment rate of 92%. Genes with more than five reads per million in only two or  
730 fewer samples were eliminated from the analysis. Differential expression analysis of the  
731 remaining genes was carried out with the R Package EdgeR (Robinson et al., 2010)  
732 using a quasi-likelihood negative binomial generalized log-linear model (EdgeR  
733 function glmQLFit) (Lun et al., 2016). Genes with  $\text{FDR} < 0.05$  were selected. A  
734 complete list of identified transcripts is in Supplemental Table S1. Venn diagrams were  
735 generated with VennDiagram R package (Chen and Boutros, 2011), and the Heatmap  
736 was generated with Complex Heatmap R package (Gu et al., 2016). GO analysis was  
737 performed using DAVID bioinformatics resources (Huang et al., 2009).

738 RNA seq data from Arabidopsis Col-0 plants UV-B irradiated was obtained  
739 from Tavridou et al. (2020). FASTQ files were obtained from Gene Expression  
740 Omnibus (GEO) repository, and processed as med17 files. Statistical analysis of the  
741 overlapping differentially expressed genes was done using the R Package GeneOverlap.

742

743 qRT-PCR analysis

744

745 Analysis was done as described in Maulion et al. (2019). Briefly, Total RNA was  
746 isolated using the TRIzol reagent (Invitrogen). 0.5 to 1.0 mg of total RNA was reverse  
747 transcribed using SuperScript II reverse transcriptase (Invitrogen) and oligo (dT) as a  
748 primer. The resultant cDNA was used as for quantitative PCR amplification in a  
749 StepOne™ System apparatus (ThermoFisher Scientific), using SYBRGreen I  
750 (Invitrogen) as a fluorescent reporter and Platinum taq polymerase (Invitrogen).  
751 Transcript levels were normalized to those of the *A. thaliana* calcium-dependent protein  
752 kinase3 (Supplemental Table S4) and to values in Col-0 plants grown under control  
753 conditions in the absence of UV-B.

754

755 Coimmunoprecipitation studies and MS analysis

756

757 For coimmunoprecipitation analyses, 3 g of Arabidopsis leaves were homogenized in a  
758 buffer containing 0.4M sacrose, 10mM Tris-HCl, pH 8.0, 10mM MgCl<sub>2</sub> and 1mM  
759 phenylmethylsulfonyl fluoride (PMSF). The extract was filtered through Miracloth and  
760 next was centrifugated for 20 min at 4500xg. The pellet was resuspended in buffer 2  
761 (0.25M sacrose, 10mM Tris-HCl, pH 8.0, 10mM MgCl<sub>2</sub>, 0.15% (v/v) Triton X-100,  
762 5mM 2 mercaptoethanol and 0.1 mM PMSF). After 5 min of incubation in ice, the  
763 extract was centrifuged at 5000xg for 10 min. The pellet was resuspended in buffer 3  
764 containing 0.44 M sacrose, 25mM Tris-HCl, pH 7.6, 10mM MgCl<sub>2</sub>, 0.5% (v/v) Triton  
765 X-100 and 10mM 2-mercaptoethanol. The supernatant was discarded, and the pellet was  
766 resuspended in buffer 4 (0.44 M sacrose, 50mM Tris-HCl, pH 7, 5mM MgCl<sub>2</sub>, 20%  
767 (v/v) glycerol and 10mM 2-mercaptoethanol) and centrifuged for 10 min at 12500xg.  
768 Finally, the pellet was resuspended in 200 µl of lysis buffer (10mM Tris-HCl, pH 7.5,  
769 50mM NaCl, 0.1% (v/v) Triton X-100, 10% (v/v) glycerol and 1mM PMSF) and  
770 sonicated. Then, the extract was centrifugated at 17500xg for 15 min. After  
771 centrifugation, 1 mL of crude extract (0.75 mg of total protein) was incubated with 6 µL



772 (3 mg) of affinity-purified rabbit polyclonal antibody raised against GFP for 3 h at 4°C  
773 with gentle agitation. After this, 20 µL of protein A agarose was added, and the samples  
774 were incubated at 4°C with gentle agitation for 1 h. The agarose beads were pelleted by  
775 centrifugation and washed four times with 200 µL of lysis buffer (100 mM Tris-HCl,  
776 pH 7.5, 1 mM EDTA, 150 mM NaCl, and 1% (v/v) Triton X-100) for 5 min at 4°C and  
777 once with LNDET buffer (250 mM LiCl, 1% Nonidet P-40, 1% [w/v] deoxycholic acid,  
778 1 mM EDTA, and 10mM Tris-HCl, pH 8.0) for 5 min at 4°C. Proteins were eluted by  
779 incubation at 95°C for 5 min in 50 µL of SDS sample buffer. Samples were loaded on  
780 10% SDS-PAGE gels and run at 100 V for 15 min to allow proteins to migrate less than  
781 1 cm into the resolving gel. Gels were stained with colloidal Coomassie Brilliant Blue  
782 stain, and the immunoprecipitated protein-loaded lane was cut into one rectangular slice  
783 of less than 1 cm of height.

784 The gel slices were subjected to in-gel digestion (Link and LaBaer, 2009;  
785 <http://cshprotocols.cshlp.org/content/2009/2/pdb.prot5110.abstract>) with trypsin  
786 (porcine, side chain protected; Promega). Briefly, specific excised samples were washed  
787 once with 50% (v/v) acetonitrile in 50 mM NH<sub>4</sub>HCO<sub>3</sub> and then dehydrated with pure  
788 acetonitrile. The gel samples were next reduced with dithiothreitol (DTT; 10 mM in 25  
789 mM NH<sub>4</sub>HCO<sub>3</sub>, 65°C for 30 min) and alkylated with iodoacetamide (55 mM in 25 mM  
790 NH<sub>4</sub>HCO<sub>3</sub>, room temperature for 30 min). Then, the gel pieces were incubated with  
791 acetonitrile, and rehydrated in 50 µL of digestion buffer (12 ng mL trypsin in 25 mM  
792 NH<sub>4</sub>HCO<sub>3</sub>) After overnight digestion at 37°C, peptides were extracted once with a  
793 solution containing 66% (v/v) acetonitrile and 5% (v/v) formic acid. The supernatants  
794 were concentrated to 5 µL by centrifugation under vacuum. The digests were analyzed  
795 by capillary HPLC-MS/MS.

796

797 HPLC-MS/MS

798

799 The peptide mixtures were analyzed in data-dependent mode on a Q-Exactive HF mass  
800 spectrometer coupled to an Ultimate 3000 nanoHPLC. A volume of 4 µL of peptide  
801 samples was loaded by the LC system. Peptides were desalted online on a reverse-phase  
802 C18 cartridge using buffer A (0.1% (v/v) formic acid) as running buffer, and then  
803 resolved on a 15-cm long PepMap nanocolumn (EASY-Spray ES801, Thermo) at a  
804 flow rate of 0.3 µL/min. Peptide elution was achieved with a gradient of buffer B (100%  
805 acetonitrile containing 0.1% formic acid). Total run time was 150 min and programmed

806 as follows: 15 min column equilibration in 96% buffer A, 4% buffer B, followed by a  
807 100 min gradient from 4% buffer B to 35%. Then, a steeper gradient from 35% buffer B  
808 to 90% was carried out in 25 min. 90% buffer B was maintained for 5 min and finally,  
809 the system was allowed to reach initial conditions in 5 min.

810 For mass spectrometric analysis in the Q Exactive HF mass spectrometer, the  
811 following tune method was used: full scan spectral range from  $m/z$  375 to 1600,  
812 automatic gain control (AGC) target value set at  $3 \times 10^6$ , and a mass resolving power of  
813 120,000 for full spectra. MS/MS were analyzed in data-dependent mode with a  
814 resolution of 30,000 and an AGC target of  $5 \times 10^5$ . Up to 20 precursors were selected  
815 for dissociation in the high-energy collisional dissociation chamber using a normalized  
816 collision energy of 27. Ion selection was performed applying a dynamic exclusion  
817 window of 15 sec.

818 For protein identification, all raw LC-MS/MS data were analyzed by MaxQuant  
819 v1.6.17.0 using the Andromeda Search engine and searched against the *A. thaliana*  
820 database downloaded from Uniprot (August 2020 release with 39,346 protein  
821 sequences). Parameters for MS/MS spectra assignment were as follows: full-trypsin  
822 specificity, maximum of two missed cleavages, instrument default parameters set for  
823 Orbitrap, carbamidomethylated cysteine as a fixed modification, and oxidized  
824 methionine and N-acetylation of protein termini as variable modifications. False  
825 discovery rate at both peptide and protein levels was set to 1%. Data filtering,  
826 processing and interpretation were performed in Perseus v1.6.14.0.

827

828 Quantification of UV absorbing compounds

829

830 One-half gram of fresh leaf tissue was frozen in liquid nitrogen and ground to a powder  
831 with a mortar and pestle. The powder was extracted for 8 hr with 3 mL of acidic  
832 methanol (1% HCl in methanol), and then by a second extraction with 6 mL of  
833 chloroform and 3 mL of distilled water. The extracts were vortexed and then centrifuged  
834 2 min at  $3,000 \times g$ . UV-B absorbing compounds were quantified by absorbance at 330  
835 nm.

836

837 Statistical analysis

838

839 Statistical analysis was done using analysis of variance models (Tukey test) or  
840 alternatively Student's *t* test (Welch's *t* tests), using untransformed data.

841

#### 842 **Accession numbers**

843

844 Sequence data from this article can be found in the The Arabidopsis Information  
845 Resource under accession number At5G20170.

846

#### 847 **Acknowledgments**

848

849 M.L.F.F., P.Ce. and P.Ca. are members of the Researcher Career of the Consejo  
850 Nacional de Investigaciones Científicas y Técnicas (CONICET). M.L.F.F. and P.Ca. are  
851 Professors at UNR. M.S.G is a doctoral fellow from CONICET, and M.S. is a doctoral  
852 fellow from FONCYT. We thank María José Maymó (CEFOBI) for care in cultivating  
853 Arabidopsis plants and Mariana Giro for help in confocal microscope imaging.

854

855

#### 856 **Supplemental data**

857

858 **Supplemental Figure S1** Venn diagrams of comparisons between transcripts with  
859 altered expression in *med17* mutants and UV-B-responsive genes in Arabidopsis plants.

860

861 **Supplemental Figure S2** Analysis of *med17* and *OE med17* plants after UV-B  
862 exposure.

863

864 **Supplemental Figure S3** Representative pictures of individual WT Col-0, *med17* and  
865 *OE MED17* plants.

866

867 **Supplemental Figure S4** UV-B effect on cell proliferation in the root meristematic  
868 zone of WT Col-0, *med17* and *OE MED17* seedlings 4 days after UV-B exposure.

869

870 **Supplemental Figure S5** UV-B effect on the root meristematic zone of WT Col-0 and  
871 *med17* 1 day after UV-B exposure.

872

873 **Supplemental Figure S6** Characterization of double *med17 atr* mutant plants.

874

875 **Supplemental Figure S7** Confocal microscopy of PI stained seeds from WT Col-0,  
876 *med17*, *atr* and *med17 atr* plants.

877

878 **Supplemental Figure S8** Programmed cell death in meristematic root cells in WT Col-  
879 0, *med17*, *atr* and *med17 atr* plants 1 day after UV-B exposure.

880

881 **Supplemental Table S1** List of transcripts expressed in *med17* mutants and comparison  
882 with expression levels in WT Col-0 plants.

883

884 **Supplemental Table S2** Cluster and GO analysis of transcripts with differential  
885 expression both in *med17* mutants compared to WT plants and after UV-B exposure in  
886 WT Col-0 plants.

887

888 **Supplemental Table S3** List of potential MED17 interaction proteins enriched in the  
889 MED17-GFP IP experiments.

890

891 **Supplemental Table S4** Primers used in for the experiments described in this work.

892

893

894 **Table 1** Proteins with a putative DNA repair role enriched in the MED17-GFP IP  
895 experiments.

Protein ID	Protein name	Accession number
Q93ZX1	Replication factor C subunit 4 (RFC4)	At1g21690
Q94K07	Nucleosome assembly protein 1;3 (NAP1;3)	At5g56950
Q9CA59	NAP1-related protein 1 (NRP1)	At1g74560
Q8GUP3	Precocious Dissociation of Sisters 5 (ATPDS5C)	At4g31880
P92948	Cell division cycle 5-like protein (CDC5)	At1g09770
F4K4Y5	DEK domain-containing chromatin associated protein	At5g55660
Q9SUA1	DEK domain-containing chromatin associated protein (DEK 3)	At4g26630
Q8LC68	NAP1-related protein 2 (NRP 2)	At1g18800
Q8W1Y0	Sister chromatid cohesion 1 protein 4 (SYN 4)	At5g16270
Q9ZQ26	DNA repair ATPase-related	At2g24420
Q9SYH2	Transcription initiation factor TFIID subunit 9 (TAF9)	At1g54140
Q93ZW3	Transcription initiation factor TFIIE subunit alpha	At1g03280

896

897

898

899 **FIGURE LEGENDS:**

900

901 **Figure 1** Analysis of global gene expression differences between *med17* compared to  
902 WT plants, and WT plants exposed to UV-B radiation. A, Venn diagram of  
903 comparisons between transcripts with altered expression in *med17* mutants and UV-B-  
904 responsive genes in Arabidopsis plants. Sets of genes were selected using the criteria  
905 described in Materials and Methods. B, Heatmap comparing transcripts changed in  
906 *med17* compared to WT plants; and WT plants after UV-B exposure. The color  
907 saturation reflects the magnitude of the log<sub>2</sub> expression ratio for each transcript. C,  
908 Clusters of expression profiles. Each graph displays the mean pattern of expression of  
909 transcripts in the cluster in blue and the standard deviation of average expression  
910 (orange and grey lines). The number of transcripts in each cluster is at the top left corner  
911 of each graph. The y-axis represents log<sub>2</sub> of gene-expression levels relative to those in  
912 WT Col-0 plants under control conditions without UV-B.

913

914 **Figure 2** *med17* plants show higher UV-B sensitivity and DNA damage after UV-B  
915 than WT plants. A, Representative images of *med17* and WT Col-0 seedlings grown  
916 under light conditions and after 15 days were UV-B irradiated (UV-B) or kept under  
917 dark conditions (darkness) as described in Materials and methods. Alternatively, plants  
918 were grown under normal photoperiod (light conditions, and then kept under normal  
919 growth conditions after UV-B or kept under dark conditions. B and C, Relative CPD  
920 levels in the DNA of WT Col-0, *med17* and *OE MED17* plants grown under control  
921 conditions or immediately after a 4-h UV-B treatment under light conditions (B), or  
922 immediately after a 4-h UV-B treatment under dark conditions and 2 h after recovery in  
923 the dark or in the light to allow photorepair (C). Results represent averages  $\pm$  S.E.M. of  
924 six independent biological replicates. Different letters indicate statistically significant  
925 differences applying ANOVA test ( $P < 0.05$ ).

926

927 **Figure 3** Programmed cell death in meristematic root cells in WT Col-0, *med17* and *OE*  
928 *MED17* plants after UV-B exposure. A and B, Number of stem cells that are dead after  
929 1 day (A) or 4 days (B) of UV-B exposure in WT Col-0, *med17* and *OE MED17* roots.  
930 Results represent the average of at least 50 biological replicates  $\pm$  S.E.M. Different  
931 letters indicate statistically significant differences applying analysis of variance test ( $p$   
932  $< 0.05$ ). C, Representative images of stem cells and adjacent daughter cells from WT  
933 Col-0, *med17* and *OE MED17* seedlings that were scored for intense PI staining to  
934 count dead stem cells per root 1 day and 4 days after a UV-B treatment or under control  
935 conditions. Scale bar represents 100  $\mu$ m.

936

937 **Figure 4** UV-B effect on expression of genes that participate in UV-B responses in WT  
938 Col-0 and *med17* seedlings. Relative expression levels of *UVR2* (A), *UVR3* (B), *UVR7*  
939 (C), *FLC* (D), *ATM* (E), *ATR* (F), *SOG1* (G), *MAPK6* (H), *UVR8* (I), *HY5* (J), *CHS* (K)  
940 and *PDCD5* (L) analyzed by RT-qPCR in WT Col-0 and *med17* seedlings under control  
941 conditions or immediately after a 4 h-UV-B treatment (UV-B). Results represent the  
942 average  $\pm$  SEM. Different letters indicate statistically significant differences applying an  
943 ANOVA test ( $P < 0.05$ ). Data represent at least three biological replicate experiments.  
944 Each RT-qPCR was repeated at least three times on each biological replicate.

945

946 **Figure 5** UV-B effect on expression of genes that participate in UV-B responses in WT  
947 Col-0 and *OE MED17* seedlings. Relative expression levels of *UVR3* (A), *UVR7* (B),

948 *HY5* (C), *PDCD5* (D), *SOG1* (E), *ATR* (F) and *ATM* (G) analyzed by RT-qPCR in WT  
949 Col-0 and *OE MED17-4* seedlings under control conditions or immediately after a 4 h-  
950 UV-B treatment (UV-B). Results represent the average  $\pm$  SEM. Different letters indicate  
951 statistically significant differences applying an ANOVA test ( $P < 0.05$ ). Data represent  
952 at least three biological replicate experiments. Each RT-qPCR was repeated at least  
953 three times on each biological replicate.

954

955 **Figure 6** Characterization of DNA damage responses in double *med17 atr* mutant  
956 plants. A, Relative CPD levels in the DNA of WT Col-0, *med17*, *atr* and *med17 atr*  
957 plants immediately after a 4-h UV-B treatment under light conditions. Results represent  
958 averages  $\pm$  S.E.M. of six independent biological replicates. B, Programmed cell death in  
959 meristematic root cells in Col-0, *med17*, *atr* and *med17 atr* plants 4 days after UV-B  
960 exposure. Results represent the average of at least 50 biological replicates  $\pm$  S.E.M.  
961 Different letters indicate statistically significant differences applying analysis of  
962 variance test ( $p < 0.05$ ). C, Representative images of stem cells and adjacent daughter  
963 cells from WT Col-0, *med17*, *atr* and *med17 atr* seedlings that were scored for intense  
964 PI staining to count dead stem cells per root 4 days after a UV-B treatment or under  
965 control conditions.

966

967 **Figure 7** UV-B root meristematic zone of *med17 atr* is similarly affected by UV-B as  
968 *med17* seedlings but differently than *atr* mutants. A, Average of meristematic root zone  
969 length; C, cortex cell number; E, cortex cell length in the root meristem from WT Col-0,  
970 *med17*, *atr* and *med17 atr* seedlings after 4 days of a UV-B treatment or under control  
971 condition. B, D and F, Ratio between meristematic root zone length (B), cortex cell  
972 number (D), and cortex cell area values (F) measured after UV-B exposure vs those  
973 under control conditions are shown. Results represent the average  $\pm$  S.E.M. Different  
974 letters indicate statistically significant differences applying analysis of variance test ( $P$   
975  $< 0.05$ ).

976

977 **Figure 8** Characterization of DNA damage responses in *OE PDCD5 med17* plants. A,  
978 Relative CPD levels in the DNA of WT Col-0, *med17*, *OE PDCD5* and *OE PDCD5*  
979 *med17* plants immediately after a 4-h UV-B treatment under light conditions. Results  
980 represent averages  $\pm$  S.E.M. of six independent biological replicates. B, Programmed  
981 cell death in meristematic root cells of WT Col-0, *med17*, *OE PDCD5* and *OE PDCD5*

982 *med17* plants 1 day after UV-B exposure. Results represent the average of at least 50  
983 biological replicates  $\pm$  S.E.M. Different letters indicate statistically significant  
984 differences applying analysis of variance test ( $P < 0.05$ ).

985

986

987





## Parsed Citations

**Anders S, Theodor Py P, Huber W (2015) HTSeq—a Python framework to work with high-throughput sequencing data. *Bioinformatics* 31:166-169.**

Google Scholar: [Author Only](#) [Title Only](#) [Author and Title](#)

**Andrews S (2010) FastQC: a quality control tool for high throughput sequence data. Available online at: <http://www.bioinformatics.babraham.ac.uk/projects/fastqc>.**

Google Scholar: [Author Only](#) [Title Only](#) [Author and Title](#)

**Arongaus AB, Chen S, Pireyre M, Glöckner N, Galvão VC, Albert, A, Winkler JB, Fankhauser C, Harter K, Ulm R (2018) Arabidopsis RUP2 represses UVR8-mediated flowering in noninductive photoperiods. *Genes Dev* 32: 1332-1343.**

Google Scholar: [Author Only](#) [Title Only](#) [Author and Title](#)

**Brown BA, Cloix C, Jiang GH, Kaiserli E, Herzyk P, Kliebenstein D J, Jenkins GI (2005) A UV-B-specific signaling component orchestrates plant UV protection. *Proc Natl Acad Sci USA* 102: 18225–18230.**

Google Scholar: [Author Only](#) [Title Only](#) [Author and Title](#)

**Buendía-Monreal M, Gillmor CS (2016) Mediator: A key regulator of plant development. *Dev Biol* 419: 7-18**

Google Scholar: [Author Only](#) [Title Only](#) [Author and Title](#)

**Casati P, Gomez MS (2021) Chromatin dynamics during DNA damage and repair in plants: new roles for old players. *J Exp Bot* doi:10.1093/jxb/eraa551**

Google Scholar: [Author Only](#) [Title Only](#) [Author and Title](#)

**Cevher MA, Shi Y, Li D, Chait BT, Malik S, Roeder RG (2014) Reconstitution of active human core Mediator complex reveals a critical role of the MED14 subunit. *Nature Struct Mol Biol* 21: 1028–1034.**

Google Scholar: [Author Only](#) [Title Only](#) [Author and Title](#)

**Chen H, Boutros PC (2011) VennDiagram: a package for the generation of highly-customizable Venn and Euler diagrams in R. *BMC Bioinformatics* 12: 35.**

Google Scholar: [Author Only](#) [Title Only](#) [Author and Title](#)

**Chen Y, Qian J, You L, Zhang X, Jiao J, Liu Y, Zhao J (2018) Subunit Interaction Differences Between the Replication Factor C Complexes in Arabidopsis and Rice. *Front Plant Sci* 9:779.**

Google Scholar: [Author Only](#) [Title Only](#) [Author and Title](#)

**Clough SJ, Bent AF (1998) Floral dip: a simplified method for Agrobacterium-mediated transformation of Arabidopsis thaliana. *Plant J* 16: 735-743.**

Google Scholar: [Author Only](#) [Title Only](#) [Author and Title](#)

**Culligan KM, Robertson CE, Foreman J, Doerner P, Britt AB (2006) ATR and ATM play both distinct and additive roles in response to ionizing radiation. *Plant J* 48: 947–961.**

Google Scholar: [Author Only](#) [Title Only](#) [Author and Title](#)

**da Costa-Nunes JA, Bhatt AM, O’Shea S, West CE, Bray CM, Grossniklaus U, Dickinson HG (2006) Characterization of the three Arabidopsis thaliana RAD21 cohesins reveals differential responses to ionizing radiation. *J Exp Bot* 57: 971–983.**

Google Scholar: [Author Only](#) [Title Only](#) [Author and Title](#)

**Davoine C, Abreu IN, Khajeh K, Blomberg J, Kidd BN, Kazan K, Schenk, PM, Gerber L, Nilsson O, Moritz T, Björklund S (2017) Functional metabolomics as a tool to analyze Mediator function and structure in plants. *PLoS one* 12: e0179640.**

Google Scholar: [Author Only](#) [Title Only](#) [Author and Title](#)

**Dolan WL, Dilkes BP, Stout JM, Bonawitz ND, Chapple C (2017) Mediator Complex Subunits MED2, MED5, MED16, and MED23 Genetically Interact in the Regulation of Phenylpropanoid Biosynthesis. *Plant Cell* 29: 3269-3285.**

Google Scholar: [Author Only](#) [Title Only](#) [Author and Title](#)

**Dotto M, Casati P (2017) Developmental reprogramming by UV-B radiation in plants. *Plant Sci* 264: 96–101.**

Google Scholar: [Author Only](#) [Title Only](#) [Author and Title](#)

**Dotto M, Gomez MS, Soto MS, Casati P (2018) UV-B radiation delays flowering time through changes in the PRC2 complex activity and miR156 levels in Arabidopsis thaliana. *Plant Cell Environ* 41: 1394–1406.**

Google Scholar: [Author Only](#) [Title Only](#) [Author and Title](#)

**Eyboulet F, Cibot C, Eychenne T, Neil H, Alibert O, Werner M., Soutourina J (2013) Mediator links transcription and DNA repair by facilitating Rad2/XPG recruitment. *Genes Dev* 27: 2549-2562.**

Google Scholar: [Author Only](#) [Title Only](#) [Author and Title](#)

**Falcone-Ferreyra M. L., Pezza A, Biarc J., Burlingame A. L., Casati P (2010) Plant L10 Ribosomal Proteins Have Different Roles during Development and Translation under Ultraviolet-B Stress. *Plant Physiol* 153: 1878-1894.**

Google Scholar: [Author Only](#) [Title Only](#) [Author and Title](#)

**Falcone Ferreyra ML, Rius SP, Casati P (2012) Flavonoids: Biosynthesis, biological functions, and biotechnological applications.**

**Frontiers Plant Sci 3: 222.**

Google Scholar: [Author Only](#) [Title Only](#) [Author and Title](#)

**Falcone Ferreyra ML, Casadevall R, D'Andrea L, AbdElgawad H, Beemster GTS, Casati P (2016) AtPDCD5 Plays a Role in Programmed Cell Death after UV-B Exposure in Arabidopsis. Plant Physiol 170: 2444–2460.**

Google Scholar: [Author Only](#) [Title Only](#) [Author and Title](#)

**Furukawa T, Curtis MJ, Tominey CM, Duong YH, Wilcox BW, Aggoune D, Hays JB, Britt AB (2010) A shared DNA-damage-response pathway for induction of stem-cell death by UVB and by gamma irradiation. DNA Repair (Amst) 9: 940–948.**

Google Scholar: [Author Only](#) [Title Only](#) [Author and Title](#)

**Gruber H, Heijde M, Heller W, Albert A, Seidlitz HK, Ulm R (2010) Negative feedback regulation of UV-B–induced photomorphogenesis and stress acclimation in Arabidopsis. Proc Natl Acad Sci USA 107: 20132–20137.**

Google Scholar: [Author Only](#) [Title Only](#) [Author and Title](#)

**Gu Z, Eils R, Schlesner M (2016) Complex heatmaps reveal patterns and correlations in multidimensional genomic data. Bioinformatics 32: 2847–2849.**

Google Scholar: [Author Only](#) [Title Only](#) [Author and Title](#)

**Guglielmi B, van Berkum NL, Klapholz B, Bijma T, Boube M, Boschiero C, Bourbon HM, Holstege FC, Werner M (2004) A high resolution protein interaction map of the yeast Mediator complex. Nucleic Acids Res 32: 5379–5391.**

Google Scholar: [Author Only](#) [Title Only](#) [Author and Title](#)

**Hanawalt PC, Spivak G (2008) Transcription-coupled DNA repair: Two decades of progress and surprises. Nat Rev Mol Cell Biol 9: 958–970.**

Google Scholar: [Author Only](#) [Title Only](#) [Author and Title](#)

**Huang DW, Sherman BT, Lempicki RA (2009) Systematic and integrative analysis of large gene lists using DAVID bioinformatics resources. Nat Protoc 4:44–57.**

Google Scholar: [Author Only](#) [Title Only](#) [Author and Title](#)

**Iñigo S, Alvarez MJ, Strasser B, Califano A, Cerdán PD (2012) PFT1, the MED25 subunit of the plant Mediator complex, promotes flowering through CONSTANS dependent and independent mechanisms in Arabidopsis. Plant J 69: 601–612.**

Google Scholar: [Author Only](#) [Title Only](#) [Author and Title](#)

**Ishibashi T, Isogai M, Kiyohara H, Hosaka M, Chiku H, Koga A, Yamamoto T, Uchiyama Y, Mori Y, Hashimoto J, Ausió J, Kimura S, Sakaguchi K (2006) Higher plant RecA-like protein is homologous to RadA DNA repair 5: 80–88.**

Google Scholar: [Author Only](#) [Title Only](#) [Author and Title](#)

**Johnson RA, Conklin PA, Tjahjadi M, Missirian V, Toal T, Brady SM, Britt AB (2018) SUPPRESSOR OF GAMMA RESPONSE1 Links DNA Damage Response to Organ Regeneration. Plant Physiol 176: 1665–1675.**

Google Scholar: [Author Only](#) [Title Only](#) [Author and Title](#)

**Kikuchi Y, Umemura H, Nishitani S, Iida S, Fukasawa R, Hayashi H, Hirose Y, Tanaka A, Sugawara K, Ohkuma Y (2015) Human mediator MED17 subunit plays essential roles in gene regulation by associating with the transcription and DNA repair machineries. Genes Cells 20: 191–202.**

Google Scholar: [Author Only](#) [Title Only](#) [Author and Title](#)

**Kim D, Langmead B, Salzberg SL (2015) HISAT: a fast spliced aligner with low memory requirements. Nature Methods 12: 357–360.**

Google Scholar: [Author Only](#) [Title Only](#) [Author and Title](#)

**Kim S, Xu X, Hecht A, Boyer TG (2006) Mediator is a transducer of Wnt/ $\beta$ -catenin signaling. J Biol Chem 281: 14066–14075.**

Google Scholar: [Author Only](#) [Title Only](#) [Author and Title](#)

**Kim YH, Zheng B, Yu Y, Won SY, Mo B, Chen X (2011) The role of Mediator in small and long noncoding RNA production in Arabidopsis thaliana. EMBO J 30: 814–822.**

Google Scholar: [Author Only](#) [Title Only](#) [Author and Title](#)

**Kong L, Chang C (2018) Suppression of wheat TaCDK8/TaWN1 interaction negatively affects germination of Blumeria graminis f. sp. tritici by interfering with very-long-chain aldehyde biosynthesis. Plant Mol Biol 96: 165–178.**

Google Scholar: [Author Only](#) [Title Only](#) [Author and Title](#)

**Lahari T, Lazaro J, Schroeder DF (2018) RAD4 and RAD23/HMR contribute to arabidopsis UV tolerance. Genes 9: 8.**

Google Scholar: [Author Only](#) [Title Only](#) [Author and Title](#)

**Lario L, Ramirez-Parra E, Gutierrez C, Casati P, Spampinato CS (2011). Regulation of plant MSH2 and MSH6 genes in the UV-B-induced DNA damage response. J Exp Bot 62: 2925–2937.**

Google Scholar: [Author Only](#) [Title Only](#) [Author and Title](#)

**Lario L, Ramirez-Parra E, Gutierrez C, Spampinato CS, Casati P (2013) ASF1 Proteins are involved in UV-induced DNA damage repair and are cell cycle regulated by E2F transcription factors in Arabidopsis thaliana. Plant Physiol 162: 1164–1177.**

Google Scholar: [Author Only](#) [Title Only](#) [Author and Title](#)

**Lin Z, Yin K, Wang X, Liu M, Chen Z, Gu H, Qu L-J (2007) Virus induced gene silencing of AtCDC5 results in accelerated cell death in**

**Arabidopsis leaves. Plant Physiol Biochem 45, 87-94.**

Google Scholar: [Author Only](#) [Title Only](#) [Author and Title](#)

**Link AJ, LaBaer J (2009) In-Gel Trypsin Digest of Gel-Fractionated Proteins. Cold Spring Harbour Protocols doi:10.1101/pdb.prot5110.**

Google Scholar: [Author Only](#) [Title Only](#) [Author and Title](#)

**Liu H, Liu B, Zhao C, Pepper M, Lin C (2011) The action mechanisms of plant cryptochromes. Trends Plant Sci 16: 684–691.**

Google Scholar: [Author Only](#) [Title Only](#) [Author and Title](#)

**Lun ATL, Chen Y, Smyth GK (2016) It's DE-licious: A Recipe for Differential Expression Analyses of RNA-seq Experiments Using Quasi-Likelihood Methods in edgeR. Methods Mol Biol 1418: 391-416.**

Google Scholar: [Author Only](#) [Title Only](#) [Author and Title](#)

**Maji S, Dahiya P, Waseem M, Dwivedi N, Bhat DS, Dar TH, Thakur JK (2019) Interaction map of Arabidopsis Mediator complex expounding its topology. Nucleic Acids Res 47: 3904–3920.**

Google Scholar: [Author Only](#) [Title Only](#) [Author and Title](#)

**Malik N, Agarwal P, Tyagi A (2017) Emerging functions of multi-protein complex Mediator with special emphasis on plants. Crit Rev Biochem Mol Biol 52: 475-502.**

Google Scholar: [Author Only](#) [Title Only](#) [Author and Title](#)

**Mao X, Weake VM, Chapple C (2019) Mediator function in plant metabolism revealed by large-scale biology. J Exp Bot 70: 5995–6003.**

Google Scholar: [Author Only](#) [Title Only](#) [Author and Title](#)

**Martínez-Trujillo M., Méndez-Bravo A, Ortiz-Castro R, Hernández-Madrigal F, Ibarra-Laclette E, Ruiz-Herrera LF, Long TA, Cervantes C, Herrera-Estrella L, López-Bucio J (2014) Chromate alters root system architecture and activates expression of genes involved in iron homeostasis and signaling in Arabidopsis thaliana. Plant Mol Biol 86: 35–50.**

Google Scholar: [Author Only](#) [Title Only](#) [Author and Title](#)

**Maulión E, Gómez MS, Falcone Ferreyra ML, Bustamante CA, Casati P (2019) AtCAF-1 mutants show different DNA damage responses after ultraviolet-B than those activated by other genotoxic agents in leaves. Plant Cell Environ 42: 2730-2745.**

Google Scholar: [Author Only](#) [Title Only](#) [Author and Title](#)

**Michaels SD, Amasino RM (1999) FLOWERING LOCUS C encodes a novel MADS domain protein that acts as a repressor of flowering. Plant Cell 11: 949–56.**

Google Scholar: [Author Only](#) [Title Only](#) [Author and Title](#)

**Murr R, Loizou JI, Yang YG, Cuenin C, Li H, Wang ZQ, Herceg Z (2006) Histone acetylation by Trrap-Tip60 modulates loading of repair proteins and repair of DNA double-strand breaks. Nat Cell Biol 8: 91–99.**

Google Scholar: [Author Only](#) [Title Only](#) [Author and Title](#)

**Nakajima S, Sugiyama M, Iwai S, Hitomi K, Otsu E, Kim S-T, Jiang C-Z, Todo T, Britt AB, Yamamoto K (1998) Cloning and characterization of a gene (UVR3) required for photorepair of 6–4 photoproducts in Arabidopsis thaliana. Nucleic Acids Res 26: 638–644.**

Google Scholar: [Author Only](#) [Title Only](#) [Author and Title](#)

**Pokorny R, Klar T, Hennecke U, Carell T, Batschauer A, Essen L-O (2008) Recognition and repair of UV lesions in loop structures of duplex DNA by DASH-type cryptochrome. Proc Natl Acad Sci USA 105: 21023–21027.**

Google Scholar: [Author Only](#) [Title Only](#) [Author and Title](#)

**Pradillo M, Knoll A, Oliver C, Varas J, Corredor E, Puchta H and Santos JL (2015) Involvement of the Cohesin Cofactor PDS5 (SPO76) During Meiosis and DNA Repair in Arabidopsis thaliana. Front Plant Sci 6: 1034.**

Google Scholar: [Author Only](#) [Title Only](#) [Author and Title](#)

**Raya-Gonzalez J, Oropeza-Aburto A, Lopez-Bucio JS, Guevara-Garcia AA, de Veylder L, Lopez-Bucio J, Herrera-Estrella L (2018) MEDIATOR18 influences Arabidopsis root architecture, represses auxin signaling and is a critical factor for cell viability in root meristems. Plant J 96: 895–909.**

Google Scholar: [Author Only](#) [Title Only](#) [Author and Title](#)

**Robinson MD, Oshlack A (2010) A scaling normalization method for differential expression analysis of RNA-seq data. Genome Biol 11: R25.**

Google Scholar: [Author Only](#) [Title Only](#) [Author and Title](#)

**Robinson MD, McCarthy DJ, Smyth GK (2010) edgeR: a Bioconductor package for differential expression analysis of digital gene expression data. Bioinformatics 26: 139-140.**

Google Scholar: [Author Only](#) [Title Only](#) [Author and Title](#)

**Ruiz-Aguilar B, Raya-González J, Salvador López-Bucio J, Reyes de la Cruz H, Herrera-Estrella L, Francisco Ruiz-Herrera F, Martínez-Trujillo M, López-Bucio J (2020) Mutation of MEDIATOR 18 and chromate trigger twinning of the primary root meristem in Arabidopsis. Plant Cell Environ 43: 1989-1999.**

Google Scholar: [Author Only](#) [Title Only](#) [Author and Title](#)

**Selby CP, Sancar A (2006) A cryptochrome/photolyase class of enzymes with single-stranded DNA-specific photolyase activity. Proc Natl Acad Sci USA 103: 17696–17700.**

Google Scholar: [Author Only](#) [Title Only](#) [Author and Title](#)

**Smaczniak C, Li N, Boeren S, America T, van Dongen W, Goerdayal SS, de Vries S, Angenent GC, Kaufmann K (2012) Proteomics-based identification of low-abundance signaling and regulatory protein complexes in native plant tissues. *Nat Prot* 7: 2144–2158.**

Google Scholar: [Author Only](#) [Title Only](#) [Author and Title](#)

**Sorek N, Szemenyei H, Sorek H, Landers A, Knight H, Bauer S, Wemmer DE, Somerville CR (2015) Identification of MEDIATOR16 as the Arabidopsis COBRA suppressor MONGOOSE1. *Proc Natl Acad Sci USA* 112: 16048-16053.**

Google Scholar: [Author Only](#) [Title Only](#) [Author and Title](#)

**Spampinato CP (2017) Protecting DNA from errors and damage: an overview of DNA repair mechanisms in plants compared to mammals. *Cel Mol Life Sci* 74: 1693-1709.**

Google Scholar: [Author Only](#) [Title Only](#) [Author and Title](#)

**Stout J, Romero-Severson E, Ruegger MO, Chapple C (2008) Semidominant mutations in reduced epidermal fluorescence 4 reduce phenylpropanoid content in Arabidopsis. *Genetics* 178: 2237-2251.**

Google Scholar: [Author Only](#) [Title Only](#) [Author and Title](#)

**Tavidou E, Pireyre M, Ulm R (2020) Degradation of the transcription factors PIF4 and PIF5 under UV-B promotes UVR8-mediated inhibition of hypocotyl growth in Arabidopsis. *Plant J* 101: 507-517.**

Google Scholar: [Author Only](#) [Title Only](#) [Author and Title](#)

**Tissot N, Ulm R (2020) Cryptochrome-mediated blue-light signalling modulates UVR8 photoreceptor activity and contributes to UV-B tolerance in Arabidopsis. *Nat Comm* 11: 1323.**

Google Scholar: [Author Only](#) [Title Only](#) [Author and Title](#)

**Ulm R, Baumann A, Oravec A, Máté Z, Adám E, Oakeley EJ, Schäfer E, Nagy F (2004) Genome-wide analysis of gene expression reveals function of the bZIP transcription factor HY5 in the UV-B response of Arabidopsis. *Proc Natl Acad Sci U S A* 101:1397-1402.**

Google Scholar: [Author Only](#) [Title Only](#) [Author and Title](#)

**Waidmann S, Kusenda B, Mayerhofer J, Mechtler K, Jonak C (2014) A DEK Domain-Containing Protein Modulates Chromatin Structure and Function in Arabidopsis. *Plant Cell* 26: 4328–4344.**

Google Scholar: [Author Only](#) [Title Only](#) [Author and Title](#)

**Wang X, Wang Q, Han Y-J, Liu Q, Gu L, Yang Z, Su J, Liu B, Zuo Z, He W, Wang J, Liu B, Matsui M, Kim J-I, Yoshito O, Lin C (2017) A CRY–BIC negative-feedback circuitry regulating blue light sensitivity of Arabidopsis. *Plant J* 92: 426–436.**

Google Scholar: [Author Only](#) [Title Only](#) [Author and Title](#)

**Xu L, Chen Y, Song Q, Xu D, Wang Y, Ma D (2009) PDCD5 interacts with Tip60 and functions as a cooperator in acetyltransferase activity and DNA damage-induced apoptosis. *Neoplasia* 11: 345–354.**

Google Scholar: [Author Only](#) [Title Only](#) [Author and Title](#)

**Yang Y, Li L, Qu LJ (2016) Plant Mediator complex and its critical functions in transcription regulation. *J Integr Plant Biol* 58: 106-118.**

Google Scholar: [Author Only](#) [Title Only](#) [Author and Title](#)

**Zhang S, Xie M, Ren G, Yu B (2013) CDC5, a DNA binding protein, positively regulates posttranscriptional processing and/or transcription of primary microRNA transcripts. *Proc Natl Acad Sci USA* 110: 17588-17593.**

Google Scholar: [Author Only](#) [Title Only](#) [Author and Title](#)

**Zheng Z, Guan H, Leal F, Grey PH, Oppenheimer DG (2013) Mediator Subunit18 Controls Flowering Time and Floral Organ Identity in Arabidopsis. *Plos One* 8: e53924.**

Google Scholar: [Author Only](#) [Title Only](#) [Author and Title](#)

**Zhu Y, Schluttenhoffer CM, Wang P, Fu F, Thimmapuram J, Zhu JK, Lee SY, Yun DJ, Mengiste T (2014) CYCLIN-DEPENDENT KINASE8 differentially regulates plant immunity to fungal pathogens through kinase-dependent and-independent functions in Arabidopsis. *Plant Cell* 26: 4149-4170.**

Google Scholar: [Author Only](#) [Title Only](#) [Author and Title](#)

**Zhuge C, Chang Y, Li Y, Chen Y, Lei J (2011) PDCD5-regulated cell fate decision after ultraviolet-irradiation-induced DNA damage. *Biophys. J* 101: 2582–2591.**

Google Scholar: [Author Only](#) [Title Only](#) [Author and Title](#)